Mechanobiological Stability of Biological Soft Tissues

Marcos Latorre[a,*], Jay D. Humphrey[a,b]

[a] *Department of Biomedical Engineering*
Yale University, New Haven, CT 06520, USA
[b] *Vascular Biology and Therapeutics Program*
Yale School of Medicine, New Haven, CT 06520, USA

Abstract

Like all other materials, biological soft tissues are subject to general laws of physics, including those governing mechanical equilibrium and stability. In addition, however, these tissues are able to respond actively to changes in their mechanical and chemical environment. There is, therefore, a pressing need to understand such processes theoretically. In this paper, we present a new rate-based constrained mixture formulation suitable for studying mechanobiological equilibrium and stability of soft tissues exposed to transient or sustained changes in material composition or applied loading. These concepts are illustrated for canonical problems in arterial mechanics, which distinguish possible stable versus unstable mechanobiological responses. Such analyses promise to yield insight into biological processes that govern both health and disease progression.

Keywords: mechanical homeostasis, extracellular matrix, adaptation, matrix turnover, tissue growth

1. Introduction

Biological soft tissues consist of myriad proteins, glycoproteins, and glycosaminoglycans (Hynes and Naba 2012), each having individual natural (stress-free) configurations, mechanical properties, and rates of turnover. It is appropriate, therefore, to consider mixture theories of multiple solid constituents when establishing theoretical frameworks for mathematically modeling growth (changes in mass) and remodeling (changes in microstructure). Adopting

*Corresponding author
Email addresses: marcos.latorre@yale.edu (Marcos Latorre), jay.humphrey@yale.edu (Jay D. Humphrey)

a classical continuum theory of mixtures presents numerous challenges, however, including difficulty in identifying constitutive relations for linear momentum exchanges between constituents as they turnover and challenges in prescribing how traction boundary conditions partition by constituent, particularly as they evolve. For this reason, we have advocated a constrained mixture theory wherein one assumes that structurally significant constituents possess individual natural configurations but are constrained to move with the mixture as a whole, and one satisfies full mixture equations for mass balance but classical equations for linear momentum balance augmented with a rule-of-mixture relation for the stored energy (Humphrey and Rajagopal 2002). Such models simplify the constitutive formulation and solution of initial-boundary value problems. Nevertheless, the full constrained mixture theory involves heredity integrals for the evolution of constituent-specific mass density and stress, which can render the associated computational modeling expensive except in problems defined by simple geometries. Rate-based models can thus be useful.

It is also well-known that biological soft tissues grow and remodel in response to changes in mechanical loading. Such responses – that is, changes in microstructural composition and/or organization and thus changes in mechanical properties and geometry – stem from mechanobiological processes, often changes in gene expression that control the production and removal of constituents in potentially evolving configurations (Humphrey et al. 2014). In parallel to classical concepts of mechanical equilibrium and mechanical stability, modeling biological growth and remodeling (G&R) necessitates an understanding of mechanobiological equilibrium and mechanobiological stability. The former can be defined by a balanced production and removal of stressed constituents within an unchanging configuration (Latorre and Humphrey 2018b); the latter can be defined as the ability of a tissue to preserve its mechanobiological equilibrium despite transient perturbations in loading under physiological or pathophysiological conditions (Cyron and Humphrey 2014). For example, we do not expect a muscle to grow or remodel simply because of a transient loading. Rather, we expect a muscle to grow or remodel in response to sustained or repetitive loading, which could lead to mechanobiological adaptivity to the new mechanical environment. Failed adaptivity can occur in disease and injury, however, which may result from a loss of mechanobiological stability.

In this paper, we first summarize a full hereditary integral-based constrained mixture model for growth and remodeling of soft tissues. We then derive a fully three-dimensional rate-based constrained mixture theory that is equivalent to the integral-based model. We subsequently particularize this formulation to a prototypical cylindrical artery to identify equilibrium solutions for vanishing rates and to assess their mechanobiological (static) stability with respect to sustained changes in external loads or model parameters. Finally, we use this rate-based approach to assess whether a (dynamic, self-excited) G&R process around a previously equilibrated solution is mechanobiologically unstable or stable, either neutrally or asymptotically, with respect to perturbations in external loads that are eventually sustained over time. For purposes of illustration, we consider computational results for a cylindrical murine aorta exposed to sustained or transient changes in mechanical loading and/or material properties. Consistent with most prior constitutive descriptions of arterial mechanics, we assume an underlying pseudoelastic rather than viscoelastic or poroelastic material response; similarly, consistent with most prior stress analyses, we assume quasi-static solutions rather than elastodynamics over a cardiac cycle (Humphrey 2002). In this way, we focus primarily on evolving mechanobiologically induced changes in geometry and material properties. Finally, we do not consider further complications associated with aortic dissection or rupture, which necessarily require one to invoke additional constitutive frameworks.

2. Theoretical Framework

2.1. Constrained mixture framework: Integral form

Consider the Cauchy stress $\boldsymbol{\sigma}$, at G&R time s, for a biological soft tissue consisting of a mixture of N structurally significant constituents and exhibiting incompressible behavior under transient mechanical loading,

$$\boldsymbol{\sigma}(s) = \sum_{\alpha=1}^{N} \boldsymbol{\sigma}^{\alpha}(s) - p(s)\,\mathbf{I} \tag{1}$$

with $\boldsymbol{\sigma}^{\alpha}$ the mixture-level contribution to $\boldsymbol{\sigma}$ of constituent $\alpha = 1, ..., N$ and p the Lagrange multiplier that enforces transient incompressibility although the tissue may change mass and

volume over G&R timescales. The stress tensor $\boldsymbol{\sigma}^{\alpha}$ can be expressed in constrained mixture models (Humphrey and Rajagopal 2002) through the following hereditary integral (Latorre and Humphrey 2018b)

$$\boxed{\boldsymbol{\sigma}^{\alpha}(s) = \frac{1}{\rho}\int_{-\infty}^{s} m^{\alpha}(\tau)\, q^{\alpha}(s,\tau)\, \hat{\boldsymbol{\sigma}}^{\alpha}(s,\tau)\, d\tau} \tag{2}$$

where ρ is the assumed constant spatial mass density of the tissue (since most of the structurally significant constituents are hydrated similarly), $m^{\alpha}(\tau) > 0$ is a spatial mass density production rate of constituent α, $q^{\alpha}(s,\tau) \in [0,1]$ is a survival function for constituent α deposited within extant matrix at G&R time $\tau \leq s$ that survives at G&R time s, and $\hat{\boldsymbol{\sigma}}^{\alpha}(s,\tau)$ is the constituent-level Cauchy stress at s for constituent α deposited at τ. Let $\hat{W}^{\alpha}(\mathbf{C}^{\alpha}_{n(\tau)}(s))$ be the strain energy function of constituent α, with $\mathbf{C}^{\alpha}_{n(\tau)}(s) = \mathbf{F}^{\alpha T}_{n(\tau)}(s)\, \mathbf{F}^{\alpha}_{n(\tau)}(s)$ the right Cauchy–Green tensor at time s for constituent α deposited at time τ, which is computed from the associated deformation gradient $\mathbf{F}^{\alpha}_{n(\tau)}(s)$ with respect to natural configuration $\kappa^{\alpha}_{n}(\tau)$, which is denoted $n(\tau)$. It can be shown that (Baek et al. 2006)

$$\mathbf{F}^{\alpha}_{n(\tau)}(s) = \mathbf{F}(s)\, \mathbf{F}^{-1}(\tau)\, \mathbf{G}^{\alpha}(\tau) \tag{3}$$

with $\mathbf{F}$ the deformation gradient of the mixture at time s or τ, measured with respect to an original homeostatic (reference) configuration $\kappa(0)$ (Figure 1), and $\mathbf{G}^{\alpha}(\tau)$ a symmetric ($\mathbf{G}^{\alpha} = \mathbf{G}^{\alpha T}$) and volume-preserving ($\det \mathbf{G}^{\alpha} = 1$) deposition (pre)stretch tensor by which constituent α is deposited within the extant matrix at time τ relative to its own possibly evolving natural configuration $\kappa^{\alpha}_{n}(\tau)$ (Figure 1). This deposition stretch arises via synthetic cells acting on the secreted matrix via actomyosin activity (Humphrey et al. 2014), thus its magnitude becomes a constitutive parameter and so too the orientation of the new tissue when deposited (Baek et al. 2006; Valentín et al. 2013). Furthermore, let the constituent-level Cauchy stress for each constituent α be

$$\hat{\boldsymbol{\sigma}}^{\alpha}(s,\tau) = \frac{2}{J^{\alpha}_{n(\tau)}(s)} \mathbf{F}^{\alpha}_{n(\tau)}(s)\, \frac{\partial \hat{W}^{\alpha}(\mathbf{C}^{\alpha}_{n(\tau)}(s))}{\partial \mathbf{C}^{\alpha}_{n(\tau)}(s)}\, \mathbf{F}^{\alpha T}_{n(\tau)}(s) \tag{4}$$

where $J^{\alpha}_{n(\tau)}(s) = \det \mathbf{F}^{\alpha}_{n(\tau)}(s) = J(s)\,/J(\tau)$, with $J = \det \mathbf{F}$ at time s or τ.

Also let ρ^{α} represent the spatial (apparent) mass density of constituent α (i.e., its mass per unit current volume of mixture) so that the assumed constant spatial mass density ρ of the mixture is

$$\rho \equiv \rho(s) = \sum_{\alpha=1}^{N} \rho^{\alpha}(s) \ . \tag{5}$$

The referential mass density $\rho_R(s) = J(s)\,\rho(s) \equiv J(s)\,\rho$ of the mixture (i.e., mass per unit reference volume) can similarly be expressed as

$$\rho_R(s) = \sum_{\alpha=1}^{N} \rho^{\alpha}_R(s) \ , \tag{6}$$

with $\rho^{\alpha}_R(s) = J(s)\,\rho^{\alpha}(s)$. Consistent with Eq. (2), $\rho^{\alpha}_R(s)$ reads in constrained mixture models (Latorre and Humphrey 2018b)

$$\boxed{\rho^{\alpha}_R(s) = \int_{-\infty}^{s} m^{\alpha}_R(\tau)\, q^{\alpha}(s,\tau)\, d\tau} \tag{7}$$

with $m^{\alpha}_R(\tau) = J(\tau)\, m^{\alpha}(\tau)$ the corresponding referential mass density production rate of constituent α. Note from Eqs. (2) and (7) that one must specify constitutive relations for $q^{\alpha}(s,\tau)$, $m^{\alpha}_R(\tau)$, and $\hat{W}^{\alpha}(\mathbf{C}^{\alpha}_{n(\tau)}(s))$ for the particular soft tissue under study.

Following previous studies of arterial G&R (Baek et al. 2007b; Latorre and Humphrey 2018b; Valentín and Humphrey 2009), we let the degradation of structural constituents be described by first-order type kinetics

$$q^{\alpha}(s,\tau) = \exp\left(-\int_{\tau}^{s} k^{\alpha}(t)\, dt\right) \tag{8}$$

where k^{α} is a rate-type parameter for mass removal that may depend on biomechanical or biochemical factors. For illustrative purposes, let (Latorre and Humphrey 2018b)

$$k^{\alpha}(t) = k^{\alpha}_o \left(1 + (\Delta\sigma(t))^2\right) \ , \quad t \in [\tau, s] \tag{9}$$

with k^{α}_o the original homeostatic value and $\Delta\sigma$ the relative difference of a given coordinate

invariant measure $\tilde{\sigma}$ of the Cauchy stress $\boldsymbol{\sigma}$ with respect to its original homeostatic value $\tilde{\sigma}_o$, namely

$$\Delta\sigma(t) = \frac{\tilde{\sigma}(t) - \tilde{\sigma}_o}{\tilde{\sigma}_o} \, . \tag{10}$$

Moreover, let the mass density production rate $m_R^\alpha(\tau)$ be described by (Latorre and Humphrey 2018b)

$$m_R^\alpha(\tau) = k^\alpha(\tau)\, \rho_R^\alpha(\tau)\, \Upsilon^\alpha(\tau) \tag{11}$$

where $k^\alpha(\tau)\, \rho_R^\alpha(\tau) =: m_N^\alpha(\tau)$ represents an evolving nominal mass production rate of constituent α per unit total reference volume and $\Upsilon^\alpha(\tau)$ is a stimulus function for G&R that can be modulated by biomechanical stimuli (e.g., in healthy arteries; Latorre and Humphrey 2018a,b; Valentín and Humphrey 2009) or other effects, as, for example, biochemical mediators or inflammation (Baek et al. 2007b; Latorre and Humphrey 2018c; Miller et al. 2014). Importantly for the present case wherein we consider mechanobiological stability of previously equilibrated mechanobiological states, m_R^α, as given in Eq. (11), should ensure a production that balances removal in any evolved homeostatic states "h" with $\Upsilon_h^\alpha \to 1$ and hence $\rho_{Rh}^\alpha \to m_{Rh}^\alpha / k_h^\alpha$. Of course, $\Upsilon_o^\alpha \equiv 1$ and $\rho_{Ro}^\alpha \equiv m_{Ro}^\alpha / k_o^\alpha$ in the original homeostatic state "o".

2.2. Constrained mixture framework: Rate form

Consider now the rate of change of the referential mass density ρ_R^α given in Eq. (7), which yields, by the Leibniz integral rule,

$$\dot{\rho}_R^\alpha(s) = m_R^\alpha(s)\, q^\alpha(s,s)\, \frac{ds}{ds} + \int_{-\infty}^{s} m_R^\alpha(\tau)\, \frac{\partial q^\alpha(s,\tau)}{\partial s} d\tau \tag{12}$$

or, upon consideration of chain and Leibniz rules in Eq. (8), (Latorre and Humphrey 2018b)

$$\boxed{\dot{\rho}_R^\alpha(s) = k^\alpha(s)\, \rho_R^\alpha(s)\, (\Upsilon^\alpha(s) - 1)} \tag{13}$$

where $q^\alpha(s,s) = 1$ and we used Eq. (11). Thus, Eq. (13) along with

$$\dot{\rho}_R(s) = \sum_{\alpha=1}^{N} \dot{\rho}_R^\alpha(s) \tag{14}$$

are equivalent to Eqs. (7) and (6), respectively, though in rate form. For later use, since $\rho_R(s) = J(s)\,\rho$, with ρ constant, note the rate of change

$$\frac{\dot{J}(s)}{J(s)} = \frac{\dot{\rho}_R(s)}{\rho_R(s)} = \sum_{\alpha=1}^{N} k^\alpha(s)\,\frac{\rho_R^\alpha(s)}{\rho_R(s)}\,(\Upsilon^\alpha(s)-1) = \sum_{\alpha=1}^{N} k^\alpha(s)\,\phi^\alpha(s)\,(\Upsilon^\alpha(s)-1) \tag{15}$$

with $\phi^\alpha := \rho^\alpha/\rho$ the spatial mass fraction of constituent α, where in this case, $\rho^\alpha/\rho \equiv \rho_R^\alpha/\rho_R$.

Evolution of the stress given by Eqs. (1) and (2) can also be described by an equivalent rate form. Consider

$$\dot{\boldsymbol{\sigma}}(s) = \sum_{\alpha=1}^{N} \dot{\boldsymbol{\sigma}}^\alpha(s) - \dot{p}(s)\,\mathbf{I} \tag{16}$$

where $\dot{\boldsymbol{\sigma}}^\alpha$ yields, from Eq. (2) and the Leibniz rule,

$$\begin{aligned}\dot{\boldsymbol{\sigma}}^\alpha(s) = &\frac{m^\alpha(s)\,q^\alpha(s,s)\,\hat{\boldsymbol{\sigma}}^\alpha(s,s)}{\rho}\frac{ds}{ds} \\ &+ \frac{1}{\rho}\int_{-\infty}^{s} m^\alpha(\tau)\,\frac{\partial q^\alpha(s,\tau)}{\partial s}\hat{\boldsymbol{\sigma}}^\alpha(s,\tau)\,d\tau \\ &+ \frac{1}{\rho}\int_{-\infty}^{s} m^\alpha(\tau)\,q^\alpha(s,\tau)\,\frac{\partial \hat{\boldsymbol{\sigma}}^\alpha(s,\tau)}{\partial s}d\tau\end{aligned} \tag{17}$$

which, with $q^\alpha(s,s) = 1$, $\partial q^\alpha(s,\tau)/\partial s = -k^\alpha(s)\,q^\alpha(s,\tau)$, $m^\alpha(s) = k^\alpha(s)\,\rho^\alpha(s)\,\Upsilon^\alpha(s)$, and a (potentially evolving) deposition Cauchy stress at the constituent level (cf. Eq. (4)) $\hat{\boldsymbol{\sigma}}^\alpha(s,s) = \mathbf{G}^\alpha(s)\,\hat{\mathbf{S}}^\alpha(\mathbf{G}^{\alpha 2}(s))\mathbf{G}^\alpha(s) = \hat{\boldsymbol{\sigma}}_{dep}^\alpha(s)$, reads

$$\begin{aligned}\dot{\boldsymbol{\sigma}}^\alpha(s) = &\,k^\alpha(s)\,\Upsilon^\alpha(s)\,\boldsymbol{\sigma}_{dep}^\alpha(s) - k^\alpha(s)\,\boldsymbol{\sigma}^\alpha(s) \\ &+ \frac{1}{\rho}\int_{-\infty}^{s} m^\alpha(\tau)\,q^\alpha(s,\tau)\,\frac{\partial \hat{\boldsymbol{\sigma}}^\alpha(s,\tau)}{\partial s}d\tau\end{aligned} \tag{18}$$

where we define the current deposition stress at the mixture level as $\boldsymbol{\sigma}_{dep}^\alpha(s) = \phi^\alpha(s)\,\hat{\boldsymbol{\sigma}}_{dep}^\alpha(s)$.

Regarding the third term in the right-hand side of Eq. (18), $\partial\hat{\boldsymbol{\sigma}}^\alpha(s,\tau)/\partial s$ yields, from

Eq. (4) (with the notation $\dot{\mathbf{F}}^{\alpha}_{n(\tau)}(s) = \partial \mathbf{F}^{\alpha}_{n(\tau)}(s)\,/\partial s$ and $\dot{J}^{\alpha}_{n(\tau)}(s) = \partial J^{\alpha}_{n(\tau)}(s)\,/\partial s$)

$$\begin{aligned}\frac{\partial \hat{\boldsymbol{\sigma}}^{\alpha}(s,\tau)}{\partial s} &= \frac{1}{J^{\alpha}_{n(\tau)}(s)}\dot{\mathbf{F}}^{\alpha}_{n(\tau)}(s)\,\hat{\mathbf{S}}^{\alpha}(\mathbf{C}^{\alpha}_{n(\tau)}(s))\mathbf{F}^{\alpha T}_{n(\tau)}(s)\\ &+ \frac{1}{J^{\alpha}_{n(\tau)}(s)}\mathbf{F}^{\alpha}_{n(\tau)}(s)\,\hat{\mathbf{S}}^{\alpha}(\mathbf{C}^{\alpha}_{n(\tau)}(s))\dot{\mathbf{F}}^{\alpha T}_{n(\tau)}(s)\\ &+ \frac{1}{J^{\alpha}_{n(\tau)}(s)}\mathbf{F}^{\alpha}_{n(\tau)}(s)\odot\mathbf{F}^{\alpha}_{n(\tau)}(s) : \frac{\partial \hat{\mathbf{S}}^{\alpha}(\mathbf{C}^{\alpha}_{n(\tau)}(s))}{\partial s}\\ &- \frac{\dot{J}^{\alpha}_{n(\tau)}(s)}{J^{\alpha 2}_{n(\tau)}(s)}\mathbf{F}^{\alpha}_{n(\tau)}(s)\,\hat{\mathbf{S}}^{\alpha}(\mathbf{C}^{\alpha}_{n(\tau)}(s))\mathbf{F}^{\alpha T}_{n(\tau)}(s)\end{aligned} \tag{19}$$

which involves the rates $\dot{\mathbf{F}}^{\alpha}_{n(\tau)}(s)$, $\dot{J}^{\alpha}_{n(\tau)}(s)$ and $\partial \hat{\mathbf{S}}^{\alpha}(\mathbf{C}^{\alpha}_{n(\tau)}(s))/\partial s$, where $\hat{\mathbf{S}}^{\alpha}(\mathbf{C}^{\alpha}_{n(\tau)}(s)) = 2\partial \hat{W}^{\alpha}/\partial \mathbf{C}^{\alpha}_{n(\tau)}(s)$, and (for further convenience) the symbol $\odot$ represents $(\mathbf{A}\odot\mathbf{B})_{ijkl} = A_{ik}B_{jl}$ while the symbol : represents the usual double contraction operation between second- or higher-order tensors, e.g., $\mathbf{A} : \mathbf{B} = A_{ij}B_{ij}$. First, from Eq. (3)

$$\dot{\mathbf{F}}^{\alpha}_{n(\tau)}(s) := \frac{\partial \mathbf{F}^{\alpha}_{n(\tau)}(s)}{\partial s} = \dot{\mathbf{F}}(s)\,\mathbf{F}^{-1}(\tau)\,\mathbf{G}^{\alpha}(\tau) = \mathbf{l}(s)\,\mathbf{F}^{\alpha}_{n(\tau)}(s) \tag{20}$$

where $\mathbf{l}(s) = \dot{\mathbf{F}}(s)\,\mathbf{F}^{-1}(s)$ is the spatial velocity gradient at the mixture level at current G&R time s. With $J^{\alpha}_{n(\tau)}(s) = J(s)\,/J(\tau)$, we have

$$\dot{J}^{\alpha}_{n(\tau)}(s) := \frac{\partial J^{\alpha}_{n(\tau)}(s)}{\partial s} = \frac{\dot{J}(s)}{J(\tau)} = \frac{\dot{J}(s)}{J(s)}J^{\alpha}_{n(\tau)}(s) \tag{21}$$

where $\dot{J}(s) = J(s)\,\mathrm{tr}\,\mathbf{l}(s)$. Moreover, the chain rule yields

$$\frac{\partial \hat{\mathbf{S}}^{\alpha}(\mathbf{C}^{\alpha}_{n(\tau)}(s))}{\partial s} = 2\frac{\partial \hat{\mathbf{S}}^{\alpha}(\mathbf{C}^{\alpha}_{n(\tau)}(s))}{\partial \mathbf{C}^{\alpha}_{n(\tau)}(s)} : \frac{\partial \mathbf{C}^{\alpha}_{n(\tau)}(s)}{\partial \mathbf{C}(s)} : \frac{1}{2}\dot{\mathbf{C}}(s)\ , \tag{22}$$

where we identify the referential constitutive (hyperelastic) fourth-order tangent tensor at the constituent level

$$\hat{\mathbb{C}}^{\alpha}(\mathbf{C}^{\alpha}_{n(\tau)}(s)) := 2\frac{\partial \hat{\mathbf{S}}^{\alpha}(\mathbf{C}^{\alpha}_{n(\tau)}(s))}{\partial \mathbf{C}^{\alpha}_{n(\tau)}(s)} = 4\frac{\partial^2 \hat{W}^{\alpha}(\mathbf{C}^{\alpha}_{n(\tau)}(s))}{\partial \mathbf{C}^{\alpha}_{n(\tau)}(s)\otimes\partial \mathbf{C}^{\alpha}_{n(\tau)}(s)} \tag{23}$$

with the symbol $\otimes$ representing $(\mathbf{A}\otimes\mathbf{B})_{ijkl}=A_{ij}B_{kl}$, and the purely kinematic fourth-order tensor (Latorre and Humphrey 2018b)

$$\frac{\partial \mathbf{C}^{\alpha}_{n(\tau)}(s)}{\partial \mathbf{C}(s)} = \mathbf{G}^{\alpha}(\tau)\,\mathbf{F}^{-T}(\tau)\odot\mathbf{G}^{\alpha}(\tau)\,\mathbf{F}^{-T}(\tau)\ . \tag{24}$$

Hence, knowing that the rate of deformation tensor $\mathbf{d}=\operatorname{sym}\mathbf{l}=\frac{1}{2}\mathbf{F}^{-T}\dot{\mathbf{C}}\mathbf{F}^{-1}$, we have, from Eq. (22), along with Eqs. (23) and (24),

$$\frac{\partial \hat{\mathbf{S}}^{\alpha}(\mathbf{C}^{\alpha}_{n(\tau)}(s))}{\partial s} = \hat{\mathbb{C}}^{\alpha}(\mathbf{C}^{\alpha}_{n(\tau)}(s)) : \mathbf{F}^{\alpha T}_{n(\tau)}(s)\odot\mathbf{F}^{\alpha T}_{n(\tau)}(s) : \mathbf{d}(s)\ . \tag{25}$$

Defining a spatial constitutive (hyperelastic) fourth-order tangent tensor $\hat{\mathbb{c}}^{\alpha}$ through the following push-forward operation over $\hat{\mathbb{C}}^{\alpha}$ at the constituent level

$$\hat{\mathbb{c}}^{\alpha}(s,\tau) = \frac{1}{J^{\alpha}_{n(\tau)}(s)}\mathbf{F}^{\alpha}_{n(\tau)}(s)\odot\mathbf{F}^{\alpha}_{n(\tau)}(s) : \hat{\mathbb{C}}^{\alpha}(\mathbf{C}^{\alpha}_{n(\tau)}(s)) : \mathbf{F}^{\alpha T}_{n(\tau)}(s)\odot\mathbf{F}^{\alpha T}_{n(\tau)}(s)\ , \tag{26}$$

then Eq. (19), with Eqs. (20), (21), and (25), reads

$$\frac{\partial \hat{\boldsymbol{\sigma}}^{\alpha}(s,\tau)}{\partial s} = \mathbf{l}(s)\,\hat{\boldsymbol{\sigma}}^{\alpha}(s,\tau) + \hat{\boldsymbol{\sigma}}^{\alpha}(s,\tau)\,\mathbf{l}^{T}(s) + \hat{\mathbb{c}}^{\alpha}(s,\tau) : \mathbf{d}(s) - \frac{\dot{J}(s)}{J(s)}\hat{\boldsymbol{\sigma}}^{\alpha}(s,\tau)\ . \tag{27}$$

Finally, substitution of Eq. (27) into Eq. (18) yields the rate equation

$$\boxed{\begin{aligned}\dot{\boldsymbol{\sigma}}^{\alpha}(s) = k^{\alpha}(s)\,\Upsilon^{\alpha}(s)\,\boldsymbol{\sigma}^{\alpha}_{dep}(s) - k^{\alpha}(s)\,\boldsymbol{\sigma}^{\alpha}(s) + \mathbb{c}^{\alpha}(s) : \mathbf{d}(s)\\ + \mathbf{l}(s)\,\boldsymbol{\sigma}^{\alpha}(s) + \boldsymbol{\sigma}^{\alpha}(s)\,\mathbf{l}^{T}(s) - \boldsymbol{\sigma}^{\alpha}(s)\operatorname{tr}\mathbf{l}(s)\end{aligned}} \tag{28}$$

where we used Eq. (2) to obtain mixture-level stresses $\boldsymbol{\sigma}^{\alpha}(s)$ from constituent-level stresses $\hat{\boldsymbol{\sigma}}^{\alpha}(s,\tau)$ and, in parallel, we defined associated mixture-level moduli $\mathbb{c}^{\alpha}$ in terms of constituent-level moduli $\hat{\mathbb{c}}^{\alpha}(s,\tau)$ through the hereditary integral

$$\mathbb{c}^{\alpha}(s) := \frac{1}{\rho}\int_{-\infty}^{s} m^{\alpha}(\tau)\,q^{\alpha}(s,\tau)\,\hat{\mathbb{c}}^{\alpha}(s,\tau)\,d\tau\ . \tag{29}$$

Eq. (28) reveals multiple contributions to the (instantaneous) change of stress $\boldsymbol{\sigma}^{\alpha}$ at G&R

time s that are intrinsically included in Eq. (2), but can only be distinguished in rate form. The first two addends associate, respectively, with an increase in stress $\boldsymbol{\sigma}^{\alpha}$ over time due to the deposition at rate $k^{\alpha}\Upsilon^{\alpha}$ of mass (cf. Eq. (13)) having prestress $\boldsymbol{\sigma}^{\alpha}_{dep}$ and removal at rate k^{α} of constituent α (cf. Eq. (13)) having stress $\boldsymbol{\sigma}^{\alpha}$, hence emphasizing the importance of rates of true production (by deposition) and removal (by degradation or death). The third addend includes material nonlinearities described constitutively by the spatial (linearized) stiffness tensor $\mathbb{c}^{\alpha}$. The fourth and fifth addends include well-known geometric nonlinearities associated with instantaneous changes of the reference configuration for the Cauchy stress (i.e., as given by $\mathbf{l}$, see Eq. (20)). Finally, the sixth addend highlights a change in stress associated with a change in current total volume (consequently, total mass) of the soft tissue over G&R timescales, as given constitutively by Eq. (15) in a coupled manner (recall that stimulus functions Υ^{α} are typically driven by stress). We assume that such mass addition occurs interstitially due to local cellular synthesis and secretion.

Remark 1

An important (yet controversial) issue that can arise when developing evolution equations directly in rate form is selection of *an* appropriate objective (i.e., frame indifferent) rate in which a spatial quantity (typically, stress) is expressed and how it relates to kinematic and/or physical quantities and their objective rates (Simó and Pister 1984). In this regard, observe that the expression for $\dot{\boldsymbol{\sigma}}^{\alpha}$ in Eq. (28) is not objective. Note, however, that we did not posit a constitutive equation for $\dot{\boldsymbol{\sigma}}^{\alpha}$; rather we obtained the (non-objective) material time derivative of the (objective) integral-type expression for $\boldsymbol{\sigma}^{\alpha}$ given in Eq. (2). In other words, both equations (Eq. (2), and Eq. (28) including all terms) describe the same evolution for $\boldsymbol{\sigma}^{\alpha}$ over G&R time s, hence we can write Eq. (28) as *a* proper objective rate of the stress tensor $\boldsymbol{\sigma}^{\alpha}$. Recalling the Truesdell rate (cf. Holzapfel 2000, p. 195), here written for each constituent α,

$$\overset{\circ}{\boldsymbol{\sigma}}{}^{\alpha}(s) = \dot{\boldsymbol{\sigma}}^{\alpha}(s) - \mathbf{l}(s)\,\boldsymbol{\sigma}^{\alpha}(s) - \boldsymbol{\sigma}^{\alpha}(s)\,\mathbf{l}^{T}(s) + \boldsymbol{\sigma}^{\alpha}(s)\,\mathrm{tr}\,\mathbf{l}(s) \tag{30}$$

allows us to write Eq. (28) as

$$\mathring{\boldsymbol{\sigma}}^{\alpha}(s) = k^{\alpha}(s)\left[\Upsilon^{\alpha}(s)\,\boldsymbol{\sigma}^{\alpha}_{dep}(s) - \boldsymbol{\sigma}^{\alpha}(s)\right] + \mathbb{c}^{\alpha}(s) : \mathbf{d}(s) \tag{31}$$

which is now an objective equation for the rate of change of mixture level Cauchy stresses $\boldsymbol{\sigma}^{\alpha}$ whose (convolution-type) solution is given, equivalently, by Eq. (2). Of course, other objective (e.g., Oldroyd/Lie, Green–Naghdi, or Jaumann) rates would give different expressions for the same constitutive relation in rate form (i.e., the expanded Eq. (28)). Equations (13) and (31), for example, thus constitute a pair of objective equations in rate form equivalent to Eqs. (7) and (2), respectively, given in (hereditary) integral form.

Remark 2

Noting that $J\boldsymbol{\sigma}^{\alpha} = \mathbf{F}\mathbf{S}^{\alpha}\mathbf{F}^{T}$, with $\mathbf{S}^{\alpha}$ the second Piola–Kirchhoff stress tensor for constituent α at the mixture level (Latorre and Humphrey 2018b), Eq. (30) can be expressed in terms of the material time derivative of $\mathbf{S}^{\alpha}$ as

$$\mathring{\boldsymbol{\sigma}}^{\alpha}(s) = \frac{1}{J(s)}\mathbf{F}(s)\,\dot{\mathbf{S}}^{\alpha}(s)\,\mathbf{F}^{T}(s) \tag{32}$$

so, from Eq. (31),

$$\dot{\mathbf{S}}^{\alpha}(s) = k^{\alpha}(s)\left[\Upsilon^{\alpha}(s)\,\mathbf{S}^{\alpha}_{dep}(s) - \mathbf{S}^{\alpha}(s)\right] + \mathbb{C}^{\alpha}(s) : \frac{1}{2}\dot{\mathbf{C}}(s) \tag{33}$$

where we defined $\mathbf{S}^{\alpha}_{dep}$ and $\mathbb{C}^{\alpha}$ through respective pull-back operations over $\boldsymbol{\sigma}^{\alpha}_{dep}$ and $\mathbb{c}^{\alpha}$, namely the Piola transformations

$$\mathbf{S}^{\alpha}_{dep}(s) := J(s)\,\mathbf{F}^{-1}(s)\,\boldsymbol{\sigma}^{\alpha}_{dep}(s)\,\mathbf{F}^{-T}(s) \tag{34}$$

and

$$\mathbb{C}^{\alpha}(s) := J(s)\,\mathbf{F}^{-1}(s) \odot \mathbf{F}^{-1}(s) : \mathbb{c}^{\alpha}(s) : \mathbf{F}^{-T}(s) \odot \mathbf{F}^{-T}(s)\ . \tag{35}$$

With Eq. (33) (equivalently, Eq. (31)) written in this way, we define (cf. Eq. (13))

$$\dot{\mathbf{S}}_g^\alpha(s) := k^\alpha(s)\left[\Upsilon^\alpha(s) - 1\right]\mathbf{S}^\alpha(s) = \frac{\dot{\rho}_R^\alpha(s)}{\rho_R^\alpha(s)}\mathbf{S}^\alpha(s) \tag{36}$$

and

$$\begin{aligned}\dot{\mathbf{S}}_r^\alpha(s) &:= -k^\alpha(s)\,\Upsilon^\alpha(s)\left[\mathbf{S}^\alpha(s) - \mathbf{S}_{dep}^\alpha(s)\right] \\ &= -\left[\frac{\dot{\rho}_R^\alpha(s)}{\rho_R^\alpha(s)} + k^\alpha(s)\right]\left[\mathbf{S}^\alpha(s) - \mathbf{S}_{dep}^\alpha(s)\right]\end{aligned} \tag{37}$$

as well as

$$\dot{\mathbf{S}}_e^\alpha(s) := \mathbb{C}^\alpha(s) : \frac{1}{2}\dot{\mathbf{C}}(s) \tag{38}$$

so that Eq. (33) results from the addition of three contributions, growth-type, remodeling / relaxation-type, and elastic-type, to the stress rate $\dot{\mathbf{S}}^\alpha$ (equivalently, $\overset{\circ}{\boldsymbol{\sigma}}{}^\alpha$ in Eq. (31)), namely

$$\dot{\mathbf{S}}^\alpha(s) = \dot{\mathbf{S}}_g^\alpha(s) + \dot{\mathbf{S}}_r^\alpha(s) + \dot{\mathbf{S}}_e^\alpha(s) \tag{39}$$

which, having been derived from the general (nonlinear, finite strain) constrained mixture model of Section 2.1, represents a generalization of the rate-form evolution equation employed in a temporally homogenized constrained mixture model for G&R (Cyron et al. 2016). Indeed, as done in viscoelasticity, in which strain-like (Latorre and Montáns 2015; Sidoroff 1974) or stress-like (Holzapfel 1996; Simó 1987) internal state variable approaches can be employed to formulate evolution equations in rate form, one could compute stress evolutions in Eqs. (36)-(38) using appropriate strain- or stress-based internal variables, bypassing the need to track contributions of individual structurally significant constituents over the mid- and long-term past history (e.g., via Eqs. (2) and (29)), with consequent savings in computational time and memory. Of course, different approaches to G&R (integral- or rate-based, with the latter either internal strain- or stress-based) could lead to different predictions and results and thus must be subjected to experimental validation.

2.3. A constrained mixture model for arterial G&R in rate form

For illustrative purposes, we now specialize the evolution equations for referential mass density and Cauchy stresses in rate form for a cylindrical artery in maturity that can exhibit active or passive (pseudoelastic) material behaviors. We consider three main structurally significant constituents, an elastin-dominated amorphous matrix ($\alpha = e$), oriented smooth muscle ($\alpha = m$), and oriented collagen ($\alpha = c$). We assume that elastin does not turnover during short to moderate periods of G&R (Wagenseil and Mecham 2009) while smooth muscle and collagen turnover continuously (generally within 4 to 6 months, Humphrey 2002). We further consider active and passive contributions by smooth muscle (Murtada et al. 2017).

Eq. (6), with $N = \{e, m, c\}$, reads for this constrained mixture of solid constituents as

$$\rho_R(s) = \sum_{\alpha}^{e,m,c} \rho_R^{\alpha}(s) = \rho_R^{e}(s) + \rho_R^{m}(s) + \rho_R^{c}(s) \tag{40}$$

whereas Eq. (1), under the assumption of an axisymmetric state of stress (with $\mathbf{e}_r$, $\mathbf{e}_\theta$, and $\mathbf{e}_z$ representing unit vectors in radial, circumferential, and axial directions, and using the compact notation $jj \to j$ for second- and fourth-order tensors) such that

$$\boldsymbol{\sigma}(s) = \sum_{j}^{r,\theta,z} \sigma_j(s)\ \mathbf{e}_j \otimes \mathbf{e}_j - p(s)\,\mathbf{I}\ , \tag{41}$$

reads for each (principal) component

$$\sigma_r(s) = \sigma_r^{e}(s) - p(s)\ \ , \tag{42}$$

$$\sigma_\theta(s) = \sum_{\alpha}^{e,m,c} \sigma_\theta^{\alpha}(s) + \sigma_\theta^{act}(s) - p(s)\ \ , \tag{43}$$

and

$$\sigma_z(s) = \sum_{\alpha}^{e,c} \sigma_z^{\alpha}(s) - p(s)\ \ , \tag{44}$$

where only the elastin-dominated material (which includes effects of glycosaminoglycans, often of much lower mass fraction than that of elastin) contributes to radial stress, while all three constituents (with separate passive and active terms for smooth muscle) contribute to

circumferential stress and only elastin and collagen contribute to axial stress. Assuming an axisymmetric deformation, $\mathbf{F}$ reads in terms of principal stretches

$$\mathbf{F}(s) = \sum_{j}^{r,\theta,z} \lambda_j(s)\ \mathbf{e}_j \otimes \mathbf{e}_j \tag{45}$$

where, from Figure 1, $\mathbf{F}(0) = \mathbf{F}_o = \mathbf{I}$ refers to the original homeostatic (loaded) configuration (cf. Bellini et al. 2014). Because of the constituent-specific deposition (pre)stretches, $\boldsymbol{\sigma}(0) = \boldsymbol{\sigma}_o \neq \mathbf{0}$, in general. The resulting spatial velocity gradient $\mathbf{l} = \dot{\mathbf{F}}\mathbf{F}^{-1}$ is also symmetric, hence

$$\mathbf{l}(s) \equiv \mathbf{d}(s) = \sum_{j}^{r,\theta,z} \frac{\dot{\lambda}_j(s)}{\lambda_j(s)}\, \mathbf{e}_j \otimes \mathbf{e}_j\ . \tag{46}$$

Lastly, since the principal directions of Cauchy stress remain constant over G&R time, we can also consider constant deposition stretch tensors $\mathbf{G}^\alpha(\tau) = \mathbf{G}^\alpha\ \forall\tau$ (Latorre and Humphrey 2018a,b; Valentín et al. 2013), with associated constituent-level deposition stresses $\hat{\boldsymbol{\sigma}}^\alpha = \mathbf{G}^\alpha\hat{\mathbf{S}}^\alpha(\mathbf{G}^{\alpha 2})\mathbf{G}^\alpha = \hat{\boldsymbol{\sigma}}^\alpha_{dep}$ constant as well (i.e., $\hat{\boldsymbol{\sigma}}^\alpha = \hat{\boldsymbol{\sigma}}^\alpha_o \equiv \hat{\boldsymbol{\sigma}}^\alpha_h$).

2.3.1. Elastin

Consistent with prior comments, arterial elastin is assumed to be deposited and cross-linked in the perinatal period and, due to its long half-life under normal conditions (> 25 years), not turnover in maturity. Hence, $m^e_R(s) \simeq 0$ for all $s \geq 0$ herein. Moreover, in the absence of diseases characterized by increased elastolytic activity, $q^e(s,0) \simeq 1$ over short-to-modest periods. Hence, elastin requires a different treatment within this formulation. We thus account for its contribution to the mechanical state of the artery at the initial time through an equivalent (fictitious, arising largely from prior somatic growth) deposition stretch tensor $\mathbf{G}^e(\tau = 0) = \mathbf{G}^e$

$$\mathbf{G}^e = \sum_{j}^{r,\theta,z} G^e_j\, \mathbf{e}_j \otimes \mathbf{e}_j \tag{47}$$

such that additional incremental deformations for elastin given by Eq. (3) at time s, with $\mathbf{F}(\tau = 0) = \mathbf{I}$, read

$$\mathbf{F}^e(s) := \mathbf{F}^e_{n(0)}(s) = \mathbf{F}(s)\,\mathbf{F}^{-1}(0)\,\mathbf{G}^e(0) = \mathbf{F}(s)\,\mathbf{G}^e \ . \tag{48}$$

The current mass of elastin per unit reference volume of mixture then remains constant over time, namely

$$\rho^e_R(s) = \rho^e_R(0) = \rho^e(0) = \rho^e_o \ , \tag{49}$$

which in rate form yields

$$\dot{\rho}^e_R(s) = 0 \tag{50}$$

consistent with Eq. (13) with neither production nor removal (i.e., $k^e\,(s) = 0$) for $s > 0$.

Under the same assumptions (no production, no removal), it can be shown that components of Cauchy stress for elastin, Eq. (2), specialize to (Latorre and Humphrey 2018b)

$$\sigma^e_j(s) = \phi^e(s)\,\lambda^2_j(s)\,G^{e2}_j\hat{S}^e_j(s) = \frac{\phi^e_o}{J(s)}\lambda^2_j(s)\,G^{e2}_j\hat{S}^e_j(s) \ , \quad j = r,\theta,z \tag{51}$$

where $\hat{\mathbf{S}}^e(\mathbf{C}^e(s)) = 2\partial\hat{W}^e(\mathbf{C}^e(s))/\partial\mathbf{C}^e(s)$, with $\mathbf{C}^e(s) := \mathbf{C}^e_{n(0)}(s)$. The material time derivative of $\sigma^e_j(s)$ in Eq. (51) yields

$$\dot{\sigma}^e_j(s) = [2\sigma^e_j(s) + c^e_{jj}(s)]\frac{\dot{\lambda}_j(s)}{\lambda_j(s)} + \sum_{k\neq j} c^e_{jk}(s)\,\frac{\dot{\lambda}_k(s)}{\lambda_k(s)} - \sigma^e_j(s)\,\frac{\dot{J}(s)}{J(s)} \tag{52}$$

which, again, is consistent with the general Eq. (28) without production or removal of elastin for $s > 0$, with c^e_{jk} $(j,k = r,\theta,z)$ given in Appendix A. Note that $2\sigma^e_j + c^e_{jj}$ accounts for geometrically and materially nonlinear stiffnesses in direction $\mathbf{e}_j$, as equivalently derived from a "theory of small on large" (Baek et al. 2007a), and that c^e_{jk}, with $j \neq k$, introduces a Poisson-type coupling between the stress rate $\dot{\sigma}^e_j$ and transverse stretch rate $\dot{\lambda}_k$.

2.3.2. Smooth muscle

We assume that, like collagen, smooth muscle is continuously produced (cell division) and removed (cell apoptosis), hence associated referential mass densities and Cauchy stresses in rate form are given by the general formulation of Section 2.2. In contrast to Eq. (50) for

elastin, Eq. (13) for smooth muscle reads

$$\dot{\rho}_R^m(s) = k^m(s)\,\rho_R^m(s)\,[\Upsilon^m(s) - 1] \ . \tag{53}$$

The deposition stretch tensor for smooth muscle, assumed to be oriented predominantly in the circumferential direction, is

$$\mathbf{G}_\theta^m = G_\theta^m\,\mathbf{e}_\theta \otimes \mathbf{e}_\theta \ , \tag{54}$$

hence the rate of change of passive circumferential stress for smooth muscle is, from Eq. (28),

$$\begin{aligned}\dot{\sigma}_\theta^m(s) = k^m(s)\,[\Upsilon^m(s)\,\phi^m(s)\,\hat{\sigma}_\theta^m - \sigma_\theta^m(s)] \\ + [2\sigma_\theta^m(s) + c_{\theta\theta}^m(s)]\,\frac{\dot{\lambda}_\theta(s)}{\lambda_\theta(s)} - \sigma_\theta^m(s)\,\frac{\dot{J}(s)}{J(s)}\end{aligned} \tag{55}$$

where $\sigma_{dep|\theta}^m(s) = \phi^m(s)\,\hat{\sigma}_\theta^m$. Note that the transverse-to-axial coupling term $c_{\theta z}^m = 0$ because smooth muscle is aligned unidirectionally (Appendix A).

2.3.3. Collagen

Consistent with prior models (Bellini et al. 2014), we consider a four-family distribution of collagen fibers, one oriented circumferentially (θ), one axially (z), and two symmetric diagonally (d). This collection of fiber families accounts for orientations observed via microscopy as well as difficult to measure cross-links that contribute to the overall anisotropy. The total referential mass density of collagen is thus

$$\rho_R^c(s) = \sum_i^{\theta,z,d} \rho_{Ri}^c(s) \tag{56}$$

which, assuming the same removal and production functions and related constants for all four families, satisfies in rate form (Latorre and Humphrey 2018b)

$$\dot{\rho}_R^c(s) = k^c(s)\,\rho_R^c(s)\,[\Upsilon^c(s) - 1] \ . \tag{57}$$

Circumferential, axial, and symmetric diagonal deposition stretches are

$$\mathbf{G}_\theta^c = G_\theta^c \, \mathbf{e}_\theta \otimes \mathbf{e}_\theta \ , \quad \mathbf{G}_z^c = G_z^c \, \mathbf{e}_z \otimes \mathbf{e}_z \ , \tag{58}$$

and

$$\mathbf{G}_d^c = G_d^c \, \mathbf{e}_d \otimes \mathbf{e}_d \ , \quad \mathbf{e}_d = \sin\alpha_d \, \mathbf{e}_\theta + \cos\alpha_d \, \mathbf{e}_z \ , \quad \text{with} \quad \alpha_d = \pm\alpha_o \ , \tag{59}$$

hence circumferential and axial components of rates of change of Cauchy stress are, from Eq. (28),

$$\begin{aligned} \dot\sigma_\theta^c(s) &= k^c(s) \left[\Upsilon^c(s) \, \phi^c(s) \, \hat\sigma_\theta^c - \sigma_\theta^c(s) \right] \\ &\quad + \left[2\sigma_\theta^c(s) + c_{\theta\theta}^c(s) \right] \frac{\dot\lambda_\theta(s)}{\lambda_\theta(s)} + c_{\theta z}^c(s) \, \frac{\dot\lambda_z(s)}{\lambda_z(s)} - \sigma_\theta^c(s) \, \frac{\dot J(s)}{J(s)} \ , \end{aligned} \tag{60}$$

and

$$\begin{aligned} \dot\sigma_z^c(s) &= k^c(s) \left[\Upsilon^c(s) \, \phi^c(s) \, \hat\sigma_z^c - \sigma_z^c(s) \right] \\ &\quad + \left[2\sigma_z^c(s) + c_{zz}^c(s) \right] \frac{\dot\lambda_z(s)}{\lambda_z(s)} + c_{z\theta}^c(s) \, \frac{\dot\lambda_\theta(s)}{\lambda_\theta(s)} - \sigma_z^c(s) \, \frac{\dot J(s)}{J(s)} \end{aligned} \tag{61}$$

where (symmetric) coupling stiffness terms $c_{\theta z}^c = c_{z\theta}^c$ persist because of the diagonal fibers (Appendix A) that contribute to σ_θ^c (along with circumferential fibers) and σ_z^c (along with axial fibers).

2.3.4. Active stress

Consider the tensile stress generated by active contraction of smooth muscle cells, which, similar to the passive stress contribution, can be expressed in the general form

$$\sigma_\theta^{act}(s) = \phi^m(s) \, \hat\sigma_\theta^{act}(s) \ . \tag{62}$$

Anticipating that we will assess mechanobiological stability of previously mechanobiologically equilibrated states, we assume the following form for $\sigma_\theta^{act}(s)$ in terms of an active second Piola–Kirchhoff stress (cf., Eq. (51) for elastin, without considering deposition stretches for the active contribution)

$$\sigma_\theta^{act}(s) = \phi^m(s)\,\hat{\sigma}_\theta^{act}(s) = \phi^m(s)\,\lambda_\theta^2(s)\,\hat{S}_\theta^{act}(s) \tag{63}$$

which does not incorporate possible time-dependent readjustment of actomyosin filament overlap to optimize the force–length response (Baek et al. 2007b), as assumed by Valentín et al. (2013). Yet, Eq. (63) allows $\hat{S}_\theta^{act}$ to depend on a ratio of vasoconstrictors to vasodilators C, as, for example

$$\sigma_\theta^{act}(s) = \phi^m(s)\,\lambda_\theta^2(s)\,\hat{S}_\theta^{act}(s) = \phi^m(s)\,\lambda_\theta^2(s)\,\hat{S}\left(1 - e^{-C^2(s)}\right) \tag{64}$$

with $\hat{S}$ a material constant and C ultimately depending on the flow-induced shear stress τ_w over the endothelium through the linearized expression (Valentín and Humphrey 2009)

$$C(s) = C_B - C_S \Delta\tau_w(s) \ , \tag{65}$$

with C_B and C_S constants, where $\Delta\tau_w$, the relative change in τ_w with respect to the original homeostatic value τ_{wo}, can be expressed in terms of associated volumetric blood flow rates (Q, Q_o) and luminal radii (a, a_o) as (Latorre and Humphrey 2018a,b)

$$\Delta\tau_w(s) = \frac{\tau_w(s) - \tau_{wo}}{\tau_{wo}} = \frac{Q(s)\,a_o^3}{Q_o a^3(s)} - 1 \ . \tag{66}$$

Inclusion of the wall shear stress here reminds us that certain components of Cauchy stress can be important mechanobiologically though not important mechanically; note that flow-induced wall shear stress is typically of the order 1.5 Pa while the pressure-induced in-plane intramural stresses are of the order 150 kPa, yet Pa-order changes in wall shear stress can dramatically affect matrix turnover and the geometry in which such turnover occurs. Nevertheless, the material time derivative of σ_θ^{act} in (63) yields, with $\phi^m = \rho^m/\rho \equiv \rho_R^m/\rho_R$,

$$\begin{aligned}\dot{\sigma}_\theta^{act}(s) = &\left(\frac{\dot{\rho}_R^m(s)}{\rho_R^m(s)} - \frac{\dot{\rho}_R(s)}{\rho_R(s)}\right)\sigma_\theta^{act}(s) \\ &+ 2\sigma_\theta^{act}(s)\,\frac{\dot{\lambda}_\theta(s)}{\lambda_\theta(s)} + \phi^m(s)\,\lambda_\theta^2(s)\,\frac{d\hat{S}_\theta^{act}(C(s))}{dC(s)}\dot{C}(s)\end{aligned} \tag{67}$$

where $\dot{C}$ reads, from Eqs. (65) and (66),

$$\dot{C}(s) = -C_S \frac{\dot{\tau}_w(s)}{\tau_{wo}} = C_S \frac{\tau_w(s)}{\tau_{wo}} \left(3\frac{\dot{a}(s)}{a(s)} - \frac{\dot{Q}(s)}{Q(s)} \right) \ . \tag{68}$$

Let an active stiffness-like term $c^{act}_{\theta\theta} > 0$ be

$$c^{act}_{\theta\theta}(s) := \phi^m(s)\, \lambda^2_\theta(s)\, 3C_S \frac{\tau_w(s)}{\tau_{wo}} \frac{d\hat{S}^{act}_\theta(C(s))}{dC(s)} \tag{69}$$

and the circumferential stretch for active stresses be approximated by

$$\lambda_\theta(s) \approx \frac{a(s)}{a_o} \tag{70}$$

so $\dot{a}/a \approx \dot{\lambda}_\theta/\lambda_\theta$, such that Eq. (67) adopts a similar expression to its passive counterpart, Eq. (55),

$$\begin{aligned} \dot{\sigma}^{act}_\theta(s) = {} & k^m(s) \left[\Upsilon^m(s)\, \phi^m(s)\, \hat{\sigma}^{act}_\theta(s) - \sigma^{act}_\theta(s) \right] \\ & + \left[2\sigma^{act}_\theta(s) + c^{act}_{\theta\theta}(s) \right] \frac{\dot{\lambda}_\theta(s)}{\lambda_\theta(s)} - \sigma^{act}_\theta(s) \frac{\dot{J}(s)}{J(s)} - \frac{c^{act}_{\theta\theta}(s)}{3} \frac{\dot{Q}(s)}{Q(s)} \ . \end{aligned} \tag{71}$$

Note that an increase (or decrease) in blood flow would potentially lead to an instantaneous vessel dilatation (or constriction) via the relaxation (or further contraction) of its smooth muscle, as desired during acute responses to altered flow (Humphrey 2002).

2.3.5. Mixture-level constitutive relations

Noticing that we include constituents that either turnover or not and that can have different passive and active contributions as well as different spatial arrangements and orientations, the constitutive relations for total referential mass density and Cauchy stresses in rate form specialize for our prototypical artery as

$$\dot{\rho}_R(s) = \sum_\alpha^{m,c} \dot{\rho}^\alpha_R(s) = \dot{J}(s)\, \rho \ , \tag{72}$$

and

$$\dot{\sigma}_\theta(s) = \sum_{\alpha}^{e,m,c,act} \dot{\sigma}_\theta^\alpha(s) - \dot{p}(s) \ , \quad \dot{\sigma}_z(s) = \sum_{\alpha}^{e,c} \dot{\sigma}_z^\alpha(s) - \dot{p}(s) \ , \quad \dot{\sigma}_r(s) = \dot{\sigma}_r^e(s) - \dot{p}(s) \tag{73}$$

where, for notational compaction, we include the superscript *act* for active circumferential stresses within the summation over the "constituent" index α. Let the "extra" part of stress (Humphrey 2002) given by different constituents in the principal directions be denoted with superscript x as

$$\sigma_\theta^x(s) = \sum_{\alpha}^{e,m,c,act} \sigma_\theta^\alpha(s) \ , \quad \sigma_z^x(s) = \sum_{\alpha}^{e,c} \sigma_z^\alpha(s) \ , \quad \text{and} \quad \sigma_r^x(s) = \sigma_r^e(s) \tag{74}$$

with respective stiffnesses as

$$c_{\theta\theta}^x(s) = \sum_{\alpha}^{e,m,c,act} c_{\theta\theta}^\alpha(s) \ , \quad c_{zz}^x(s) = \sum_{\alpha}^{e,c} c_{zz}^\alpha(s) \ , \quad \text{and} \quad c_{rr}^x(s) = c_{rr}^e(s) \tag{75}$$

as well as (with $c_{jk}^x = c_{kj}^x$)

$$c_{\theta z}^x(s) = \sum_{\alpha}^{e,c} c_{\theta z}^\alpha(s) \ , \quad c_{zr}^x(s) = c_{zr}^e(s) \ , \quad \text{and} \quad c_{\theta r}^x(s) = c_{\theta r}^e(s) \ . \tag{76}$$

Hence, with Eqs. (53), (57) for referential mass densities, and Eqs. (52), (55), (60), (61), and (71) for stress contributions, we can write constrained mixture equations in rate form for an idealized cylindrical artery as

$$\dot{\rho}_R = \sum_{\alpha}^{m,c} k^\alpha \rho_R^\alpha \left(\Upsilon^\alpha - 1\right) \tag{77}$$

$$\dot{\sigma}_\theta + \frac{c_{\theta\theta}^{act}}{3}\frac{\dot{Q}}{Q} = \sum_{\alpha}^{m,c,act} k^\alpha \left(\Upsilon^\alpha \frac{\rho_R^\alpha}{\rho_R}\hat{\sigma}_\theta^\alpha - \sigma_\theta^\alpha\right) + 2\sigma_\theta^x \frac{\dot{\lambda}_\theta}{\lambda_\theta} + \sum_{j}^{r,\theta,z} c_{\theta j}^x \frac{\dot{\lambda}_j}{\lambda_j} - \sigma_\theta^x \frac{\dot{\rho}_R}{\rho_R} - \dot{p} \tag{78}$$

$$\dot{\sigma}_z = k^c \left(\Upsilon^c \frac{\rho_R^c}{\rho_R}\hat{\sigma}_z^c - \sigma_z^c\right) + 2\sigma_z^x \frac{\dot{\lambda}_z}{\lambda_z} + \sum_{j}^{r,\theta,z} c_{zj}^x \frac{\dot{\lambda}_j}{\lambda_j} - \sigma_z^x \frac{\dot{\rho}_R}{\rho_R} - \dot{p} \tag{79}$$

$$\dot{\sigma}_r = 2\sigma_r^x \frac{\dot{\lambda}_r}{\lambda_r} + \sum_{j}^{r,\theta,z} c_{rj}^x \frac{\dot{\lambda}_j}{\lambda_j} - \sigma_r^x \frac{\dot{\rho}_R}{\rho_R} - \dot{p} \tag{80}$$

where the rates in the right-hand sides are yet to be related to the variables of interest for each particular case. Note that these, and all relations in Section 2.3, hold at any point within a cylindrical arterial wall whether thin- or thick-walled.

2.4. Equivalent thin-walled artery: Stability analysis

We seek to analyze the mechanobiological stability of evolving loaded states of an artery, which we assume to have achieved a state of mechanobiological equilibrium when subjected to an inner pressure $P = P_h$, flow rate $Q = Q_h$, and axial stretch $\lambda_z = \lambda_{zh}$. Because these external loads are eventually sustained over time during the dynamic stability analyses performed, the resulting solutions represent self-excited deformations caused by combined growth, remodeling, and elastic responses. That is, we are not analyzing forced dynamic responses, either over short (cardiac cycle) or long (G&R) timescales. Moreover, because of residual stresses in maturity (which arise from materially non-uniform deposition stretches and somatic growth), the mean values of Cauchy stress represent well the transmural distribution of stress. Hence, we use mean values similar to those for a thin-walled pressure vessel. Because of the aforementioned order of magnitude difference in mean in-plane (θ and z) and out-of-plane (r) stresses, we also assume a quasi-plane-stress state for which $|\sigma_r|/\sigma_\theta \sim |\sigma_r|/\sigma_z \ll 1$, hence the Lagrange multiplier in Eqs. (78)-(80) is obtained directly from Eq. (42) as (hereafter, we omit any dependences on times s or τ for notational convenience)

$$\sigma_r = \sigma_r^e - p = 0 \quad \Longrightarrow \quad p = \sigma_r^e \, . \tag{81}$$

Noticing from Eq. (51) that $\sigma_j^e \propto G_j^{e2}$ and that in-plane deposition stretches for elastin are typically $G_\theta^e \sim G_z^e \sim 2$, with $G_r^e = 1/(G_\theta^e G_z^e) \sim 1/4$, we have

$$\frac{|\sigma_r^e|}{\sigma_\theta^e} \sim \frac{|\sigma_r^e|}{\sigma_z^e} \sim \left(\frac{1}{G_\theta^e G_z^e}\right)^3 \ll 1 \tag{82}$$

and because smooth muscle and/or collagen contribute to circumferential and axial stresses through Eqs. $(74)_1$ and $(74)_2$, we find

$$|p| = |\sigma_r^e| \ll \sigma_\theta^e, \sigma_z^e < \sigma_\theta^x, \sigma_z^x \tag{83}$$

whereby p will be negligible in this mechanobiological stability analysis. If this assumption did not hold at a given homeostatic (loaded) state, a similar procedure could be followed while incorporating $\dot{p} = \dot{\sigma}_r^e$, from Eq. (80), in Eqs. (78) and (79). Finally, for analytical convenience, we consider the same (original) rates and gains for turnover of smooth muscle and collagen, thus

$$k_o^m = k_o^c \equiv k_o \ , \quad \text{and} \quad \Upsilon^m = \Upsilon^c \equiv \Upsilon \ . \tag{84}$$

2.4.1. Nonlinear, non-autonomous system

The previous assumptions, along with the external loads remaining constant over time during the stability (self-excitation) analysis, that is,

$$P = P_h \ , \quad Q = Q_h \ , \quad \lambda_z = \lambda_{zh} \implies \dot{P} = 0 \ , \quad \dot{Q} = 0 \ , \quad \dot{\lambda}_z = 0 \tag{85}$$

reduce Eqs. (77)-(80) to the following nonlinear system of first-order differential equations

$$\dot{\rho}_R = k \left(\Upsilon - 1 \right) \left(\rho_R - \rho_o^e \right) \tag{86}$$

$$\dot{\sigma}_\theta = k \sum_{\alpha}^{m,c,act} \left(\Upsilon \frac{\rho_R^\alpha}{\rho_R} \hat{\sigma}_\theta^\alpha - \sigma_\theta^\alpha \right) + \left(2\sigma_\theta + c_{\theta\theta} \right) \frac{\dot{\lambda}_\theta}{\lambda_\theta} + c_{\theta r} \frac{\dot{\lambda}_r}{\lambda_r} - \sigma_\theta \frac{\dot{\rho}_R}{\rho_R} \tag{87}$$

$$\dot{\sigma}_z = k \left(\Upsilon \frac{\rho_R^c}{\rho_R} \hat{\sigma}_z^c - \sigma_z^c \right) + c_{z\theta} \frac{\dot{\lambda}_\theta}{\lambda_\theta} + c_{zr} \frac{\dot{\lambda}_r}{\lambda_r} - \sigma_z \frac{\dot{\rho}_R}{\rho_R} \tag{88}$$

which suggests that ρ_R, σ_θ, and σ_z could represent an appropriate set of time-dependent variables for an asymptotic stability analysis of arterial G&R if the three right-hand sides could be expressed as functions of these variables and, perhaps, G&R time s, either implicitly or explicitly. In other words, we seek to identify a non-autonomous system of the form (Rouche et al. 1977)

$$\dot{\mathbf{y}} \left(s \right) = \mathbf{f} \left(\mathbf{y} \left(s \right), s \right) \ , \quad s \geq 0 \ , \quad \mathbf{y} \left(0 \right) = \mathbf{y}_h + \delta \mathbf{y}_h \tag{89}$$

with $\mathbf{y} = \left[\rho_R, \sigma_\theta, \sigma_z \right]^T$ the dependent variable, s the independent variable, $\mathbf{f} \left(\mathbf{y}, s \right)$ a nonlinear vector-valued function, and $\delta \mathbf{y}_h$ an initial (typically modest) perturbation relative to the evolved homeostatic state $\mathbf{y}_h = \left[\rho_{Rh}, \sigma_{\theta h}, \sigma_{zh} \right]^T$.

Consider first the global equilibrium equation for mean circumferential stress $\sigma_\theta = Pa/h$, with transmural pressure P, luminal radius a, and wall thickness h, which can be expressed in terms of $\gamma_h = P_h/P_o$, $\sigma_{\theta o} = P_o a_o/h_o$, $\lambda_\theta = a/a_o$, and $\rho_R/\rho = J = \lambda_r\lambda_\theta\lambda_{zh}$, with $\lambda_r = h/h_o$, as

$$\sigma_\theta = \sigma_{\theta o}\frac{P_h a h_o}{P_o a_o h} = \gamma_h\sigma_{\theta o}\frac{\lambda_\theta}{\lambda_r} = \gamma_h\sigma_{\theta o}\frac{\lambda_\theta^2\lambda_{zh}}{J} = \gamma_h\lambda_{zh}\rho\sigma_{\theta o}\frac{\lambda_\theta^2}{\rho_R} \tag{90}$$

Hence, internal (constitutive) and external (mechanical equilibrium) expressions for $\dot\sigma_\theta$ yield, from Eqs. (87) and (90)

$$k\sum_\alpha^{m,c,act}\left(\Upsilon\frac{\rho_R^\alpha}{\rho_R}\hat\sigma_\theta^\alpha - \sigma_\theta^\alpha\right) + (2\sigma_\theta + c_{\theta\theta})\frac{\dot\lambda_\theta}{\lambda_\theta} + c_{\theta r}\frac{\dot\lambda_r}{\lambda_r} - \sigma_\theta\frac{\dot\rho_R}{\rho_R} = \sigma_\theta\left(2\frac{\dot\lambda_\theta}{\lambda_\theta} - \frac{\dot\rho_R}{\rho_R}\right) \tag{91}$$

whereupon the associated (total) Truesdell rate vanishes, cf. Eq. (31),

$$\mathring{\sigma}_\theta = k\sum_\alpha^{m,c,act}\left(\Upsilon\frac{\rho_R^\alpha}{\rho_R}\hat\sigma_\theta^\alpha - \sigma_\theta^\alpha\right) + c_{\theta\theta}\frac{\dot\lambda_\theta}{\lambda_\theta} + c_{\theta r}\frac{\dot\lambda_r}{\lambda_r} = 0 \tag{92}$$

Furthermore, $\dot J = J\,\mathrm{tr}\,\mathbf{l}$, with Eqs. $(15)_1$ and (46), and $\dot\lambda_z = 0$, yields

$$\frac{\dot\lambda_\theta}{\lambda_\theta} + \frac{\dot\lambda_r}{\lambda_r} = \frac{\dot\rho_R}{\rho_R} \tag{93}$$

which, along with Eq. (92), enable expressions for $\dot\lambda_\theta/\lambda_\theta$ and $\dot\lambda_r/\lambda_r$ to be substituted into Eqs. (87) and (88). Letting the stimulus function Υ in Eqs. (86)-(88) be driven by relative intramural $\Delta\sigma$ (same as in Eq. (9)) and wall shear $\Delta\tau_w$ stresses (same as in Eq. (65)) through a linearized relation (Latorre and Humphrey 2018b; Valentín and Humphrey 2009), we have

$$\Upsilon = 1 + K_\sigma\Delta\sigma - K_\tau\Delta\tau_w \tag{94}$$

with $K_\sigma \geq 0$ and $K_\tau \geq 0$ gain-type G&R parameters, and $\tilde\sigma$ in Eq. (10) the first principal invariant of $\boldsymbol{\sigma}$, namely $\sigma_I = \sigma_r + \sigma_\theta + \sigma_z \simeq \sigma_\theta + \sigma_z$, so

$$\Delta\sigma = \frac{\sigma_I - \sigma_{Io}}{\sigma_{Io}} \simeq \frac{\sigma_\theta + \sigma_z}{\sigma_{\theta o} + \sigma_{zo}} - 1 \tag{95}$$

which, importantly, accounts for the biaxial wall mechanics, noting that axial mechanics

plays fundamental roles in arterial mechanics (Humphrey et al. 2009), including arterial G&R (Gleason et al. 2007). In addition, we can rewrite τ_w/τ_{wo} in Eq. (66), with $\varepsilon_h = Q_h/Q_o$ and Eq. (90), as

$$\frac{\tau_w}{\tau_{wo}} = \frac{Q_h a_o^3}{Q_o a^3} = \frac{\varepsilon_h}{\lambda_\theta^3} = \varepsilon_h \left(\gamma_h \lambda_{zh} \frac{\rho \sigma_{\theta o}}{\rho_R \sigma_\theta} \right)^{3/2} \tag{96}$$

so we obtain the desired dependences for $\Upsilon = \Upsilon(\mathbf{y}) \equiv \Upsilon(\rho_R, \sigma_\theta, \sigma_z)$. Now, let the terms $\sum_\alpha^{m,c,act} \sigma_\theta^\alpha$ and σ_z^c in Eqs. (87) and (88) be expressed as

$$\sum_\alpha^{m,c,act} \sigma_\theta^\alpha = \sigma_\theta - \sigma_\theta^e \ , \quad \text{and} \quad \sigma_z^c = \sigma_z - \sigma_z^e \ . \tag{97}$$

If, as in previous work (Latorre and Humphrey 2018a,b,c), the hyperelastic response of elastin is modeled via a neoHookean function with shear modulus c^e, for which $\hat{S}_\theta^e = \hat{S}_z^e = c^e$ are constant, we have from Eqs. (51) and (90)

$$\sigma_\theta^e = \phi_o^e G_\theta^{e2} \hat{S}_\theta^e \frac{\lambda_\theta^2}{J} = \sigma_{\theta o}^e \frac{\lambda_\theta^2}{J} = \frac{\sigma_{\theta o}^e}{\gamma_h \lambda_{zh} \sigma_{\theta o}} \sigma_\theta \tag{98}$$

and

$$\sigma_z^e = \phi_o^e G_z^{e2} \hat{S}_z^e \frac{\lambda_{zh}^2}{J} = \sigma_{zo}^e \frac{\lambda_{zh}^2}{J} = \lambda_{zh}^2 \sigma_{zo}^e \frac{\rho}{\rho_R} \tag{99}$$

whereby terms in Eq. (97) can be expressed as a function of the variables in $\mathbf{y} = [\rho_R, \sigma_\theta, \sigma_z]^T$ as

$$\sum_\alpha^{m,c,act} \sigma_\theta^\alpha = \left(1 - \frac{\sigma_{\theta o}^e}{\gamma_h \lambda_{zh} \sigma_{\theta o}} \right) \sigma_\theta \ , \quad \text{and} \quad \sigma_z^c = \left(1 - \lambda_{zh}^2 \frac{\rho \sigma_{zo}^e}{\rho_R \sigma_z} \right) \sigma_z \ . \tag{100}$$

Likewise, because $c_{jk}^e = 0$ for this particular case, $c_{\theta r} = 0 = c_{zr}$ in Eqs. (87) and (88). Consider, finally, the terms in Eqs. (87) and (88)

$$\sum_\alpha^{m,c,act} \frac{\rho_R^\alpha}{\rho_R} \hat{\sigma}_\theta^\alpha \ , \quad \text{and} \quad \frac{\rho_R^c}{\rho_R} \hat{\sigma}_z^c \tag{101}$$

which, after noticing that if (Latorre and Humphrey 2018b)

$$k_o^m = k_o^c \ , \ \Upsilon^m = \Upsilon^c \quad \Longrightarrow \quad \frac{\rho_R^m}{\rho_o^m} = \frac{\rho_R^c}{\rho_o^c} = \frac{\rho_R^m + \rho_R^c}{\rho_o^m + \rho_o^c} = \frac{\rho_R - \rho_o^e}{\rho - \rho_o^e} \tag{102}$$

then

$$\frac{\rho_R^c}{\rho_R}\hat{\sigma}_z^c = \frac{\rho}{\rho_R}\frac{\rho_R^c}{\rho_o^c}\frac{\rho_o^c}{\rho}\hat{\sigma}_z^c = \frac{\rho}{\rho_R}\frac{\rho_R - \rho_o^e}{\rho - \rho_o^e}\sigma_{zo}^c \tag{103}$$

with the (original) total axial stress for collagen $\sigma_{zo}^c = \phi_o^\alpha \hat{\sigma}_z^c$ constant. Moreover

$$\sum_\alpha^{m,c,act} \frac{\rho_R^\alpha}{\rho_R}\hat{\sigma}_\theta^\alpha = \sum_\alpha^{m,c,act} \frac{\rho}{\rho_R}\frac{\rho_R^\alpha}{\rho_o^\alpha}\frac{\rho_o^\alpha}{\rho}\hat{\sigma}_\theta^\alpha = \frac{\rho}{\rho_R}\frac{\rho_R - \rho_o^e}{\rho - \rho_o^e}\sum_\alpha^{m,c,act} \phi_o^\alpha \hat{\sigma}_\theta^\alpha \tag{104}$$

with

$$\sum_\alpha^{m,c,act} \phi_o^\alpha \hat{\sigma}_\theta^\alpha = \phi_o^m \hat{\sigma}_\theta^m + \phi_o^c \hat{\sigma}_\theta^c + \phi_o^m \hat{\sigma}_\theta^{act} = \sigma_{\theta o}^m + \sigma_{\theta o}^c + \phi_o^m \frac{\rho_R \sigma_\theta}{\gamma_h \lambda_{zh} \rho \sigma_{\theta o}} \hat{S}_\theta^{act}\left(\sigma_\theta, \rho_R\right) \tag{105}$$

where $\sigma_{\theta o}^m$ and $\sigma_{\theta o}^c$ are constant. Note, from Eqs. (63), (64), (65), (90) and (96), the dependences for $\hat{\sigma}_\theta^{act}$

$$\hat{\sigma}_\theta^{act} = \lambda_\theta^2\left(\sigma_\theta, \rho_R\right)\hat{S}_\theta^{act}\left(\sigma_\theta, \rho_R\right) \ . \tag{106}$$

Therefore, after some lengthy (but otherwise straightforward) algebra, Eqs. (86)-(88) reduce to the following nonlinear system of differential equations of the form in Eq. (89), which, for prescribed constant loads P_h, Q_h, λ_{zh}, and initial perturbation $\delta\mathbf{y}_h$, describes the evolution of ρ_R, σ_θ, and σ_z in terms of themselves and the G&R-time-dependent stiffnesses $c_{\theta\theta}$ and $c_{z\theta}$ (see Eqs. (75), (76), and Appendix A), namely

$$\boxed{\begin{aligned}
\frac{\dot{\rho}_R}{k\rho_R} &= \frac{\rho_R - \rho_o^e}{\rho_R}\left(\Upsilon - 1\right) && (107)\\
\frac{\dot{\sigma}_\theta}{k\sigma_\theta} &= -\frac{\rho_R - \rho_o^e}{\rho_R}\left(\Upsilon - 1\right) + \frac{2\sigma_\theta}{c_{\theta\theta}}\Omega && (108)\\
\frac{\dot{\sigma}_z}{k\sigma_z} &= -\frac{\rho_R - \rho_o^e}{\rho_R}\left(\Upsilon - 1\right) + \frac{2\sigma_\theta}{c_{\theta\theta}}\frac{c_{z\theta}}{2\sigma_z}\Omega - \chi && (109)
\end{aligned}}$$

where

$$\Upsilon = 1 + K_\sigma\left(\frac{\sigma_\theta + \sigma_z}{\sigma_{\theta o} + \sigma_{zo}} - 1\right) - K_\tau\left(\frac{\tau_w}{\tau_{wo}} - 1\right) \ , \tag{110}$$

and we defined

$$\Omega := 1 - \frac{1}{\gamma_h \lambda_{zh}}\frac{\sigma_{\theta o}^e}{\sigma_{\theta o}} - \Upsilon\frac{\rho_R - \rho_o^e}{\rho - \rho_o^e}\left(\frac{\rho}{\rho_R}\frac{\sigma_{\theta o}^m + \sigma_{\theta o}^c}{\sigma_\theta} + \frac{1}{\gamma_h \lambda_{zh}}\frac{\phi_o^m \hat{S}_\theta^{act}}{\sigma_{\theta o}}\right) \ , \tag{111}$$

and

$$\chi := 1 - \lambda_{zh}^2 \frac{\rho}{\rho_R} \frac{\sigma_{zo}^e}{\sigma_z} - \Upsilon \frac{\rho_R - \rho_o^e}{\rho - \rho_o^e} \frac{\rho}{\rho_R} \frac{\sigma_{zo}^c}{\sigma_z} \tag{112}$$

with τ_w/τ_{wo} (in Υ) and $\hat{S}_\theta^{act}$ (in Ω) functions of ρ_R and σ_θ from Eqs. (96) and (106). Although one would need to update the hereditary-integral-based elastic moduli $c_{\theta\theta}$ and $c_{z\theta}$ (cf. Eq. (29)) between incremental steps to solve numerically Eqs. (107)-(109) for ρ_R, σ_θ, and σ_z, we will just need their homeostatic values $c_{\theta\theta h}$ and $c_{z\theta h}$ to analyze the stability of the dynamical system of Equations (107)-(109) near a homeostatic state.

2.4.2. Mechanobiological equilibrium

As mentioned above, we seek a mechanobiological stability analysis of an equilibrated mechanobiological state, previously computed for prescribed P_h, Q_h, λ_{zh}. Mathematically, the equilibrated state $\mathbf{y}_h$ must satisfy $\dot{\rho}_R = 0$, $\dot{\sigma}_\theta = 0$, and $\dot{\sigma}_z = 0$ in Eqs. (107)-(109), that is, from Eq. (89)

$$\mathbf{0} = \mathbf{f}\left(\mathbf{y}\left(s\right), s\right) \quad \forall s \geq 0 \quad \Longrightarrow \quad \mathbf{y}\left(s\right) = \mathbf{y}_h \tag{113}$$

hence representing a so-called *equilibrium* or *critical* point (Rouche et al. 1977) of this system of first-order differential equations.

Considering $\dot{\rho}_R|_h = 0$, $\dot{\sigma}_\theta|_h = 0$, and $\dot{\sigma}_z|_h = 0$ in Eqs. (107)-(109), requires

$$\Upsilon_h = 1 \ , \quad \Omega_h = 0 \ , \quad \text{and} \quad \chi_h = 0 \tag{114}$$

at mechanobiological equilibrium. It can be shown, numerically, that the steady-state solution $\mathbf{y}_h = [\rho_{Rh}, \sigma_{\theta h}, \sigma_{zh}]^T$ obtained from Eq. (114), via our rate-based constrained mixture approach, represents the same mechanobiologically equilibrated solution obtained from an integral-based constrained mixture approach for the same prototypical vessel (Latorre and Humphrey 2018b). In particular, it is easy to verify, analytically, that the original homeostatic rule-of-mixture solution (cf. Section 3.2 in Latorre and Humphrey (2018b), with volume and mass fractions being equivalent and p negligible with respect to in-plane stresses)

$$\rho_R = \sum_{\alpha}^{e,m,c} \rho_o^\alpha \equiv \rho \ , \tag{115}$$

$$\sigma_\theta = \sum_{\alpha}^{e,m,c,act} \phi_o^\alpha \hat{\sigma}_{\theta o}^\alpha = \sum_{\alpha}^{e,m,c,act} \sigma_{\theta o}^\alpha \equiv \sigma_{\theta o} \ , \tag{116}$$

and

$$\sigma_z = \sum_{\alpha}^{e,c} \phi_o^\alpha \hat{\sigma}_{zo}^\alpha = \sum_{\alpha}^{e,c} \sigma_{zo}^\alpha \equiv \sigma_{zo} \tag{117}$$

obtained for $P = P_o$, $Q = Q_o$, and $\lambda_z = \lambda_{zo} = 1$, satisfies $\Upsilon_o - 1 = \Omega_o = \chi_o = 0$ in Eqs. (110)-(112), and, thus, represents an associated critical point of the system of first-order Equations (107)-(109).

2.4.3. Mechanobiological stability

Importantly, distinction between time-dependent and time-independent solutions, Eqs. (89) and (113), respectively, allows us to analyze two types of (un)stable responses related to different mechanobiological sources. Briefly, Eq. (89) describes the evolution of $\mathbf{y}(s)$ near a previously mechanobiologically equilibrated solution $\mathbf{y}_h$ following an initial perturbation $\delta\mathbf{y}_h$ at $s = 0$ for prescribed model parameters and external loads for $s \geq 0$, and, hence, requires that the critical point $\mathbf{y}_h$ exists and is bounded, in general. Subsequently, a dynamic stability analysis determines if the *time-dependent* solution $\mathbf{y}(s > 0)$ approaches $\mathbf{y}_h$, remains close to $\mathbf{y}_h$, or diverges. On other hand, Eq. (113) yields a *time-independent* mechanobiologically equilibrated solution $\mathbf{y}_h$ for prescribed model parameters and external loads, which might be statically bounded or unbounded, or even give rise to bifurcations. We thus refer to mechanobiological dynamic stability as the ability of the time-dependent solution $\mathbf{y}(s)$ to remain close to a finite (bounded) equilibrated state $\mathbf{y}_h$, with rate-dependent terms in Eq. (89) playing a central role. We alternatively refer to mechanobiological static stability as the ability of time-independent solutions $\mathbf{y}_h$ to remain finite (bounded), where only rate-independent terms in Eq. (89) are relevant.

Mechanobiological (static) stability of $\mathbf{y}_h$ *with respect to sustained perturbations.* Consider our idealized artery with initial geometry and mass fractions $\mathbf{x}_o = \{a_o, h_o, l_o, \phi_o\}$ in an original homeostatic (loaded) state o. An associated original equilibrated solution $\mathbf{y}_o = [\rho_{Ro}, \sigma_{\theta o}, \sigma_{zo}]^T$ (with $\rho_{Ro} = \rho$) is obtained from Eq. (113) for prescribed original external loads $\boldsymbol{\xi}_o = \{P_o, Q_o, \lambda_{zo}\}$ and original model parameters $\boldsymbol{\varsigma}_o$, namely, Eqs. (115)-(117). Con-

sider, too, an evolved equilibrated solution $\mathbf{y}_h = [\rho_{Rh}, \sigma_{\theta h}, \sigma_{zh}]^T$, obtained from Eq. (113) for evolved loads $\boldsymbol{\xi}_h = \{P_h, Q_h, \lambda_{zh}\}$ and evolved parameters $\boldsymbol{\varsigma}_h$, which can be computed numerically from the three conditions in Eq. (114) (cf., equivalently, Latorre and Humphrey 2018b). The steady-state solution $\mathbf{y}_h$ is called mechanobiologically stable with respect to sustained changes in external loads $\boldsymbol{\xi}_h$ if, for every (physiological) $\epsilon > 0$, there is a (physiological) $\delta > 0$, such that

$$\|\boldsymbol{\xi}_h - \boldsymbol{\xi}_o\| < \epsilon \implies \|\mathbf{y}_h - \mathbf{y}_o\| < \delta \ . \tag{118}$$

Equivalently, $\mathbf{y}_h$ is called mechanobiologically stable with respect to sustained changes in parameters $\boldsymbol{\varsigma}_h$ if, for every (physiological) $\epsilon > 0$, there is a (physiological) $\delta > 0$, such that

$$\|\boldsymbol{\varsigma}_h - \boldsymbol{\varsigma}_o\| < \epsilon \implies \|\mathbf{y}_h - \mathbf{y}_o\| < \delta \ . \tag{119}$$

Otherwise, the steady-state solution $\mathbf{y}_h$ is mechanobiologically unstable with respect to physiologically admissible changes in $\boldsymbol{\xi}_h$ or $\boldsymbol{\varsigma}_h$. Note that neither G&R time s nor rate-dependent terms influence this type of statically (un)bounded solution.

Eq. (113) with $\mathbf{y}(s) = \mathbf{y}_h$, absent G&R time s, and explicit consideration of the evolution of a single parameter $\zeta_h \in \{\boldsymbol{\xi}_h, \boldsymbol{\varsigma}_h\}$ can be rewritten as a one-parameter family of equations $\mathbf{f}(\mathbf{y}_h, \zeta_h) = \mathbf{0}$. By the implicit function theorem, we have

$$\mathbf{f}(\mathbf{y}_h, \zeta_h) = \mathbf{0} \implies \mathbf{y}_h = \mathbf{y}_h(\zeta_h) \ , \tag{120}$$

hence static stability of $\mathbf{y}_h$ with respect to changes in ζ_h can be assessed through the evolution of the (implicit) parameter-dependent solution $\mathbf{y}_h = \mathbf{y}_h(\zeta_h)$. Differentiation of $\mathbf{f}(\mathbf{y}_h(\zeta_h), \zeta_h) = \mathbf{0}$ with respect to ζ_h yields

$$\frac{d\mathbf{f}(\mathbf{y}_h(\zeta_h), \zeta_h)}{d\zeta_h} = \frac{\partial \mathbf{f}(\mathbf{y}_h, \zeta_h)}{\partial \mathbf{y}_h} \cdot \frac{d\mathbf{y}_h(\zeta_h)}{d\zeta_h} + \frac{\partial \mathbf{f}(\mathbf{y}_h, \zeta_h)}{\partial \zeta_h} = \mathbf{0} \tag{121}$$

whereupon

$$\frac{d\mathbf{y}_h(\zeta_h)}{d\zeta_h} = -\left.\frac{\partial \mathbf{f}(\mathbf{y}_h, \zeta_h)}{\partial \mathbf{y}_h}\right|^{-1} \cdot \frac{\partial \mathbf{f}(\mathbf{y}_h, \zeta_h)}{\partial \zeta_h} \ . \tag{122}$$

A first-order Taylor expansion yields $\mathbf{y}_h(\zeta_h + \Delta\zeta_h) \simeq \mathbf{y}_h(\zeta_h) + (d\mathbf{y}_h(\zeta_h)/d\zeta_h)\Delta\zeta_h$. Assuming

that $\|\mathbf{y}_h\|$ increases monotonically with respect to monotonic changes in $\Delta\zeta_h$, mechanobiological static stability of $\mathbf{y}_h$, in the sense of Eqs. (118) or (119), requires, from Eq. (122), that the Jacobian matrix $\partial\mathbf{f}\left(\mathbf{y}_h,\zeta_h\right)/\partial\mathbf{y}_h$ is invertible. In other words, if there exists a physiological value ζ_h (i.e., $|\zeta_h-\zeta_o|<\epsilon$), such that

$$\det\left[\frac{\partial\mathbf{f}\left(\mathbf{y}_h,\zeta_h\right)}{\partial\mathbf{y}_h}\right]\to 0 \quad\Longrightarrow\quad \left\|\mathbf{y}_h\left(\zeta_h\right)-\mathbf{y}_o\right\|\to\infty \tag{123}$$

then the mechanobiologically equilibrated solution $\mathbf{y}_h$ is statically unstable (i.e., unbounded). For our idealized artery,

$$\frac{\partial\mathbf{f}\left(\mathbf{y}_h,\zeta_h\right)}{\partial\mathbf{y}_h}=\left.\frac{\partial\mathbf{f}\left(\mathbf{y},\zeta\right)}{\partial\mathbf{y}}\right|_h=\left[\begin{array}{ccc}\dfrac{\partial\dot{\rho}_R}{\partial\rho_R} & \dfrac{\partial\dot{\rho}_R}{\partial\sigma_\theta} & \dfrac{\partial\dot{\rho}_R}{\partial\sigma_z}\\ \dfrac{\partial\dot{\sigma}_\theta}{\partial\rho_R} & \dfrac{\partial\dot{\sigma}_\theta}{\partial\sigma_\theta} & \dfrac{\partial\dot{\sigma}_\theta}{\partial\sigma_z}\\ \dfrac{\partial\dot{\sigma}_z}{\partial\rho_R} & \dfrac{\partial\dot{\sigma}_z}{\partial\sigma_\theta} & \dfrac{\partial\dot{\sigma}_z}{\partial\sigma_z}\end{array}\right]_h \tag{124}$$

which we compute numerically using Eqs. (107)-(109) in examples below. Importantly, other types of G&R instabilities (not necessarily unbounded) could arise depending on the specific evolution of the nonlinear function $\mathbf{y}_h\left(\zeta_h\right)$, including limit-point instabilities and/or bifurcations (cf. Erlich et al. 2019). Hence, each case, defined by specific constitutive relations, material constants, geometry, and boundary conditions should be evaluated separately (Haslach and Humphrey 2004).

Mechanobiological (dynamic) stability of $\mathbf{y}\left(s\right)$ *with respect to transient perturbations near* $\mathbf{y}_h$. As explained above, a mechanobiologically equilibrated solution $\mathbf{y}_h$ represents a critical point of Eq. (89) for a given original geometry and mass fractions $\mathbf{x}_o$, prescribed evolved loads $\boldsymbol{\xi}_h$, and prescribed evolved model parameters $\boldsymbol{\varsigma}_h$. Assume now that for a given $\epsilon_h>0$, there exists a $\delta_h>0$ such that Eqs. (118) and (119) are satisfied, or, in other words, that $\mathbf{y}_h$ exists and remains physiological. Eq. (89), with $\mathbf{x}_o$ given, and $\boldsymbol{\xi}_h$ and $\boldsymbol{\varsigma}_h$ fixed, describes a time-dependent solution $\mathbf{y}\left(s\geq 0\right)$ following an initial perturbation $\delta\mathbf{y}_h$ at $s=0$. The time-dependent solution $\mathbf{y}(s)$ is called mechanobiologically stable at $s=0$ with respect to

arbitrary perturbations $\delta\mathbf{y}_h$ if, for every $\epsilon > 0$, there is a $\delta > 0$ such that if

$$\|\delta\mathbf{y}_h\| < \epsilon \implies \|\mathbf{y}(s) - \mathbf{y}_h\| < \delta \quad \forall s \geq 0 \ . \tag{125}$$

Otherwise, $\mathbf{y}(s)$ is mechanobiologically unstable at $s = 0$ with respect to transient perturbations $\delta\mathbf{y}_h$. Note that both the G&R time s and rate-dependent terms play crucial roles in dynamically (un)bounded solutions.

Consider an evolved equilibrium solution $\mathbf{y}_h = [\rho_{Rh}, \sigma_{\theta h}, \sigma_{zh}]^T$ of Eqs. (107)-(109) for prescribed $\boldsymbol{\xi}_h$ and $\boldsymbol{\varsigma}_h$, with $\dot{\mathbf{y}} = \mathbf{0}$. We linearize about $\mathbf{y}_h(0)$, as given in Eq. (89), as

$$\dot{\mathbf{y}} = \mathbf{f}(\mathbf{y}, s) \simeq \mathbf{f}(\mathbf{y}_h, 0) + \left.\frac{\partial \mathbf{f}(\mathbf{y}, s)}{\partial \mathbf{y}}\right|_h \cdot (\mathbf{y} - \mathbf{y}_h) + \left.\frac{\partial \mathbf{f}(\mathbf{y}, s)}{\partial s}\right|_h (s - 0) \tag{126}$$

where we neglect higher-order terms. Considering that $c_{\theta\theta}$ and $c_{z\theta}$ are additional variables (to ρ_R, σ_θ, and σ_z) that depend on s,

$$\left.\frac{\partial \mathbf{f}(\mathbf{y}, s)}{\partial s}\right|_h = \left[\begin{array}{c} \dfrac{\partial \dot{\rho}_R}{\partial s} \\ \dfrac{\partial \dot{\sigma}_\theta}{\partial s} \\ \dfrac{\partial \dot{\sigma}_z}{\partial s} \end{array}\right]_h = \Omega_h \left[\begin{array}{c} 0 \\ -\dfrac{2\sigma_\theta}{c_{\theta\theta}^2}\dfrac{dc_{\theta\theta}}{ds} \\ -\dfrac{2\sigma_\theta}{c_{\theta\theta}^2}\dfrac{c_{z\theta}^2}{2\sigma_z}\dfrac{d(c_{\theta\theta}/c_{z\theta})}{ds} \end{array}\right]_h = \mathbf{0} \tag{127}$$

which, importantly, vanish because of the equilibrium value $\Omega_h = 0$ in Eq. (114). Thus, since $\mathbf{y}_h$ is an equilibrium point (i.e., $\mathbf{f}(\mathbf{y}_h, 0) = \mathbf{0}$) and $\partial \mathbf{f}(\mathbf{y}, s)/\partial s|_h = \mathbf{0}$, linearization of Eq. (89) at $\mathbf{y}_h$ (i.e., Eq. (126)) is represented by a linear autonomous system of differential equations in terms of an incremental (time-dependent) solution $\delta\mathbf{y}(s) = \mathbf{y}(s) - \mathbf{y}_h$

$$\delta\dot{\mathbf{y}}(s) = \left.\frac{\partial \mathbf{f}(\mathbf{y}, s)}{\partial \mathbf{y}}\right|_h \cdot \delta\mathbf{y}(s) \ , \quad s \geq 0 \ , \quad \delta\mathbf{y}(0) = \delta\mathbf{y}_h \ , \tag{128}$$

which is valid in a neighborhood of the evolved homeostatic solution $\mathbf{y} = \mathbf{y}_h$.

It is well-known (Hairer et al. 1993) that the eigenvalues of the matrix of constant coefficients $\partial \mathbf{f}(\mathbf{y}, s)/\partial \mathbf{y}|_h$ determine the stability of the associated linear(ized), autonomous system given in Eq. (128). The question now is whether these eigenvalues determine, too, the stability of the nonlinear, non-autonomous system given in Eq. (89) near the equilibrium

state $\mathbf{y}_h$. This theory, initiated in the late 1800s, was "brought to perfection"(Hairer et al. 1993) by Lyapunov (1882), so we employ his main contributions in this regard.

Original homeostatic state. For illustration, we analyze analytically the asymptotic stability of $\mathbf{y}(s)$ near the original equilibrium state $\mathbf{y}_o$. After considering the dependences of the right-hand sides of Eqs. (107)-(109) on ρ_R, σ_θ, and σ_z, performing all the required partial derivatives in Eq. (124), and rearranging terms conveniently (see Appendix B), we obtain the following (generally complex) eigenvalues for the linearized problem of Eq. (128) particularized at the original state $\mathbf{y}_o$

$$l_{1o} = -k_o \tag{129}$$

$$l_{2o} = \frac{k_o}{2}\left(T_o + \sqrt{T_o^2 - 4D_o}\right) \tag{130}$$

$$l_{3o} = \frac{k_o}{2}\left(T_o - \sqrt{T_o^2 - 4D_o}\right) \tag{131}$$

where $T_o := (\mathrm{tr}\,(\partial\mathbf{f}/\partial\mathbf{y}|_o) - l_{1o})/k_o = \mathrm{tr}\,(\partial\mathbf{f}/\partial\mathbf{y}|_o)/k_o + 1$ reads

$$T_o = -\left(\frac{2\sigma_{\theta o}^{ne}}{c_{\theta\theta o}}\frac{\mathcal{C}_{\theta zo}}{2\sigma_{\theta o}} + \phi_o^{ne} - \phi_o^e\frac{\hat{\sigma}_{zo}^{ne}}{\sigma_{\theta o}}\right)\bar{K}_\sigma - \frac{2\sigma_{\theta o}^{ne}}{c_{\theta\theta o}}\bar{K}_\tau - \frac{\mathcal{C}_{\theta\theta o}^{act}}{c_{\theta\theta o}} + \frac{2\sigma_{\theta o}^{ne}}{c_{\theta\theta o}}\ , \tag{132}$$

and $D_o := (\det(\partial\mathbf{f}/\partial\mathbf{y}|_o)/l_{1o})/k_o^2 = -\det(\partial\mathbf{f}/\partial\mathbf{y}|_o)/k_o^3$ reads

$$D_o = \left(\frac{2\sigma_{\theta o}^{ne}}{c_{\theta\theta o}}\phi_o^e\left(1 + \frac{\hat{\sigma}_{zo}^{ne}}{\sigma_{\theta o}}\right) + \frac{\mathcal{C}_{\theta\theta o}^{act}}{c_{\theta\theta o}}\left(\phi_o^{ne} - \phi_o^e\frac{\hat{\sigma}_{zo}^{ne}}{\sigma_{\theta o}}\right)\right)\bar{K}_\sigma + \frac{2\sigma_{\theta o}^{ne}}{c_{\theta\theta o}}\bar{K}_\tau\ , \tag{133}$$

with $\bar{K}_\sigma = K_\sigma\sigma_{\theta o}/\sigma_{Io}$, $\bar{K}_\tau = 3K_\tau/2$, $\phi_o^{ne} = 1 - \phi_o^e$, $\sigma_{\theta o}^{ne} = \sigma_{\theta o} - \sigma_{\theta o}^e$, $\hat{\sigma}_{zo}^{ne} = \sigma_{zo} - \hat{\sigma}_{zo}^e$, $\mathcal{C}_{\theta zo} = 2\sigma_{\theta o} + c_{\theta zo}$, and $\mathcal{C}_{\theta\theta o}^{act} = 2\sigma_{\theta o}^{act} + c_{\theta\theta o}^{act}$. Clearly, many parameters influence the system, including mass fractions, active stress and stiffness (which can depend on vasoactive parameters), passive circumferential and axial stresses, and circumferential and axial-to-circumferential total stiffnesses (that depend, additionally, on elastic constants, deposition stretches and diagonal collagen orientation), and, of course, rate and gain parameters for removal and production.

Regarding the type and sign of the eigenvalues l_{1o} to l_{3o} in Eqs. (129)-(131), we firstly

observe that

$$k_o \gtrless 0 \implies l_{1o} \lesseqgtr 0 \ . \tag{134}$$

Hence, for $l_{1o} < 0$ (i.e., with $k_o > 0$, which is physical), one can assure, based on a linearized analysis (Rouche et al. 1977), that the following (partial) results regarding the critical point $\mathbf{y}_o = [\rho, \sigma_{\theta o}, \sigma_{zo}]^T$ of the nonlinear system of Eqs. (107)-(109) hold in a neighborhood of $\mathbf{y}_o$ (cf. the Trace-Determinant plane, Figure 9.1.9 in Boyce and DiPrima 2012) such that

$$T_o < 0 \quad \text{and} \quad D_o > 0 \implies \mathbf{y}\,(s) \text{ is asymptotically stable} \tag{135}$$

or

$$T_o > 0 \quad \text{or} \quad D_o < 0 \implies \mathbf{y}\,(s) \text{ is unstable} \tag{136}$$

where neglect of higher-order terms in Eq. (126) intentionally disregarded particular cases that would generally require their consideration (e.g., complex eigenvalues with vanishing real parts, giving rise to "the [nonlinear] center problem", cf. Hairer et al. 1993). Importantly, if, because of the current lack of empirical evidence of oscillatory behaviors in vivo over G&R timescales, one assumes that physiological G&R responses are dynamically stable and progress over time without oscillations, then $T_o < 0$ and $D_o > 0$ in Eq. (135) must additionally satisfy

$$T_o < -2\sqrt{D_o} < 0 \implies \mathbf{y}\,(s) \text{ is asymptotically stable without oscillations} \tag{137}$$

which, based on Eqs. (132) and (133), imposes conditions on mechanobiological parameters to ensure physiologically reasonable dynamical adaptations. Indeed, depending on different values of the trace T_o and determinant D_o (hence, eigenvalues l_{2o} and l_{3o}), we found in numerical examples below that so-called asymptotically stable (spiral or nodal) sinks, unstable (spiral or nodal) sources, or neutrally stable centers (Boyce and DiPrima 2012) are mathematically admissible.

2.5. Illustrative results for the murine aorta

Recall that the mechanical response of elastin is modelled using a neoHookean relation

$$\hat{W}^e(\mathbf{C}^e(s)) = \frac{c^e}{2}\left(\mathbf{C}^e(s) : \mathbf{I} - 3\right) \ , \tag{138}$$

with c^e a shear modulus, which we used to express σ_θ^e and σ_z^e in Eqs. (98) and (99) in terms of the primary variables σ_θ and ρ_R. Conversely, smooth muscle and collagen are modelled using Fung-type relations

$$\hat{W}^\alpha(\lambda^\alpha_{n(\tau)}(s)) = \frac{c_1^\alpha}{4c_2^\alpha}\left[e^{c_2^\alpha(\lambda^{\alpha 2}_{n(\tau)}(s)-1)^2} - 1\right] \ , \quad \alpha = m, c \ , \tag{139}$$

where c_1^α (dimensions of stress) and c_2^α (dimensionless) are material parameters, and $\lambda^\alpha_{n(\tau)}(s)$ is the fiber stretch (relative to its evolving natural configuration due to continued matrix production). Collagen fiber families oriented in circumferential, axial, and symmetric diagonal directions have respective fractions β_θ, β_z, and $\beta_d = 1 - \beta_\theta - \beta_z$. Representative values of parameters for a mouse descending thoracic aorta are listed in Table 1, with smooth muscle and collagen sharing rate and gain constants for convenience, recall Eqs. (84) and (94). Additional values needed to quantify the active response of smooth muscle through Eqs. (64) and (65) are given in specific examples below. The inner pressure at the original homeostatic state, for vanishing active contribution, is $P_o = 13.2\,\text{kPa}$, with mean values of circumferential $\sigma_{\theta o} = 213\,\text{kPa}$ and axial $\sigma_{zo} = 238\,\text{kPa}$ stresses in the original homeostatic state, consistent with experimental findings (Bellini et al. 2014).

3. Illustrative Results

Here, we consider three cases of (patho)physiological importance – an acute but sustained increase in blood pressure, a pathological loss of elastin, and the role of active smooth muscle contraction – as well as two studies of key constitutive parameters.

3.1. Mechanobiological stability of equilibrium solutions

3.1.1. Acute increase in pressure

Consider the equilibrium inner pressure ratio $\gamma_h = P_h/P_o$ as the driving parameter ζ_h for a one-parameter family of nonlinear equations of the type $(120)_1$, explicitly, Eqs. (107)-(109) with $\dot{\mathbf{y}} = [\dot{\rho}_R, \dot{\sigma}_\theta, \dot{\sigma}_z]^T = \mathbf{0}\ \forall s \geq 0$, or, alternatively, Eqs. (114). Let the flow rate and axial stretch preserve their original homeostatic values $\varepsilon_h = Q_h/Q_o = 1$ and $\lambda_{zh} = 1$. The solution to these time-independent equations, with baseline parameters in Table 1, represents a mechanobiologically equilibrated state for each γ_h, that is, $\mathbf{y}_h(\gamma_h)$ in Eq. $(120)_2$. Corresponding inner radius a_h, thickness h_h and axial force f_h are then obtained from $\rho_{Rh}/\rho = J_h$ plus the mechanical equilibrium equations $\sigma_{\theta h} = P_h a_h/h_h$ and $\sigma_{zh} = f_h/(2\pi a_h h_h)$, with $J_h/\lambda_{zh} = \lambda_{rh}\lambda_{\theta h} = h_h a_h/(h_o a_o)$.

Figure 2 shows equilibrium values for (a) a_h, (b) h_h, (d) $\sigma_{\theta h}$, and (e) σ_{zh} as functions of the stimulation-driver P_h/P_o. In addition, panels (c) and (f) show the evolution of these variables in respective phase-type planes, with the driving parameter γ_h removed. The pressure was increased from its original homeostatic value $\gamma_o = 1$ (i.e., $P_o \approx 99\,\text{mmHg}$) up to an evolved ratio $\gamma_h = 1.8$ (i.e., $P_h \approx 178\,\text{mmHg}$), hence $\epsilon = 0.8P_o$ in Eq. (118), which is a proper range of biological interest. Observe that all the equilibrium variables remain statically bounded for increasing pressure within this range (following, e.g., Humphrey 2002, qualitatively), which, according to Eq. (118), represents a mechanobiologically stable situation. The problem remains well-posed for this range of pressures, with the γ_h-dependent Jacobian determinant, cf. Eq. (123), $D_o = -\det(\partial\mathbf{f}/\partial\mathbf{y}|_o)/k_o^3 = 0.15$ for $\gamma_o = 1$ and $D_h = -\det(\partial\mathbf{f}/\partial\mathbf{y}|_h)/k_h^3 = 0.10$ for $\gamma_h = 1.8$. The partial derivatives $\partial\mathbf{f}/\partial\mathbf{y}|_h$ at equilibrium points $\mathbf{y}_h(\gamma_h)$, see Eq. (124), were computed numerically via forward (first-order) finite differences. In particular, the Jacobian determinant computed numerically at the original homeostatic state was consistent with the analytical expression in Eq. (133). Results show wall thickening with slight dilatation as is common in hypertension (Humphrey 2002).

3.1.2. Elastin degradation

Consider G&R driven, quasi-statically, by elastin degradation prescribed by $\zeta_h \equiv c_h^e = (1 - \varphi_h)\, c_o^e$, where c_o^e is the original shear modulus for elastin, c_h^e is the evolved modulus used

to compute the associated equilibrated states, and $\varphi_h \in [0,1]$ quantifies elastin degradation. In addition to the flow rate and axial stretch, the inner pressure also remains constant, that is, $\gamma_h = \varepsilon_h = \lambda_{zh} = 1$. Note that the modified elastin properties, Eqs. (98) and (99) derived for a constant value c^e, needed to be updated by the corresponding factor, $c^e_h/c^e_o = 1-\varphi_h$. If $K_\tau = K_\sigma/2$ (Table 1), we find a bounded growth of the vessel for all $\varphi_h \in [0,1]$; in contrast, if $K_\tau = K_\sigma/5$, we find an unbounded growth at some $\varphi_h < 1$. Specifically, Figure 3 shows equilibrium values for (a) a_h, (b) h_h, (d) $\sigma_{\theta h}$, and (e) σ_{zh} as functions of the stimulation-driver φ_h. Panels (c) and (f) show associated evolutions in phase planes. Following prior studies, which decrease either the mass fraction of elastin (Cyron et al. 2014; Zeinali-Davarani et al. 2011) or its elastic parameter (Valentín et al. 2013; Watton et al. 2004), we degraded c^e_h up to $\varphi_{h,max} \approx 0.8$, namely $\epsilon \approx 0.8 c^e_o$ in Eq. (119). Observe in this case that equilibrium values of inner radius and thickness, which remain statically bounded initially, rapidly diverge when c^e_h approaches the value $c^e_h = (1-0.775)c^e_o = 0.225c^e_o$, at which an asymptotic growth response occurs. Consistent with Eq. (123), the problem becomes ill-posed during a quasi-static evolution, with Jacobian determinants $D_o = 0.069$ for $\varphi_o = 0$ and $D_h \to 0^+$ for $\varphi_h \to 0.775^-$. Conversely, equilibrium values of intramural stresses decreased only slightly, remaining close to normal. These results are consistent with previous evolution analyses and observations (cf. Valentín et al. 2013 and references therein) showing that irreversible damage to elastin prevents an artery from maintaining its original homeostatic geometry and composition; with the passive stress contribution by elastin diminished, the artery distends and collagen production increases in an attempt to compensate (Cyron et al. 2014).

A similar asymptotic growth response results for the pressure-driven case of Figure 2, with $c^e_h = c^e_o$ constant, but with $K_\tau = K_\sigma/5$ and a high inner pressure of $P_h \approx 4.4P_o$, which could be reached only in cases of extreme adaptations such as veins placed in the arterial system (Ramachandra et al. 2017). Note that this blow-up pressure, if any, depends on specific values of material parameters. Finally, the Jacobian determinants D_h computed for all the static cases studied evolved continuously and were positive. According to Eq. (122), a potential change of sign of $D_h(\mathbf{y}_h, \zeta_h)$, occurring at a bounded equilibrium state $\mathbf{y}_h$, could lead to singularities of some primary variables in the corresponding phase plane. At least in the cases analyzed, with the present boundary conditions, constitutive relations

and simulation-driver parameters, we observed asymptotic responses and not limit points or bifurcations.

3.2. Mechanobiological stability of dynamic evolutions

3.2.1. Gain parameters K_σ and K_τ

The results in Section 3.1 describe how (static) equilibrium points of the system of Eqs. (107)-(109) evolve with respect to sustained changes in external loads or model parameters (e.g., in Figures 2 or 3). Ideally, in the absence of further perturbations, these solutions would remain statically equilibrated. We now employ Eqs. (107)-(109), including rate terms, to describe how perturbed dynamic solutions behave near a previously equilibrated point under constant loads. Specifically, consider perturbations of $\mathbf{y}\,(s)$ around the original homeostatic state $\mathbf{y}_o$ with parameters in Table 1, that is, the initial equilibrium point in Figures 2 or 3. To show a precise correspondence between the integral-based formulation of Section 2.1 and rate-based formulation of Section 2.2, we compute the eigenvalues of the Jacobian matrix in Eqs. (129)-(131) but also the temporal evolution of the system using the integral-based formulation. For all cases analyzed, the transient (impulse-like) perturbation consists of a rapid rise of inner pressure up to $1.5P_o$ at $s = 0^+$ days, which is maintained for 20 days and returned back to the original homeostatic value P_o at $s = 20^+$ days. The dynamic stability character of $\mathbf{y}\,(s)$ around the original state $\mathbf{y}_o$ is then analyzed according to Eq. (125).

Figure 4 shows five different dynamic responses associated with increasing absolute values of the gain parameters $K_\sigma = 2K_\tau > 0$, which, based on Eq. (110), do not modify the original homeostatic state (because the terms within parentheses vanish originally, i.e., $\Upsilon_o \equiv 1$ in any case). For the first case, $K_\sigma = 0.03$, we obtain $T_o = 0.149 > 0$ and $D_o = 0.004 > 0$, which yields eigenvalues $l_{2o}/k_o = 0.110 > 0$ and $l_{3o}/k_o = 0.040 > 0$ in Eqs. (130) and (131), representing an asymptotically unstable (non-oscillatory) solution, or unstable source; see the phase plane in Figure 4. The case $K_\sigma = 0.12$ yields $T_o = 0.087 > 0$ and $D_o = 0.018 > 0$, with complex conjugates l_{2o} and l_{3o} given by $R_o \equiv \mathrm{Re}(l_{2o})/k_o = 0.044 > 0$ and $I_o \equiv \mathrm{Im}(l_{2o})/k_o = 0.125$, representing an asymptotically unstable (oscillatory) solution, or unstable spiral. The specific value $K_\sigma = 0.2445$ results in a dynamic response that is neutrally stable around $\mathbf{y}_o$, with $T_o = 0$ and $D_o = 0.036 > 0$, hence $R_o = 0$ and $I_o = 0.189$, represented by a stable

center. The oscillatory response becomes asymptotically stable for a further increase up to $K_\sigma = 0.3$, with $T_o = -0.038 < 0$ and $D_o = 0.044 > 0$, hence $R_o = -0.019 < 0$ and $I_o = 0.208$, represented by a stable spiral in the phase plane. Finally, for the higher value $K_\sigma = 1.8$, we obtain $T_o = -1.075 < 0$ and $D_o = 0.262 > 0$, which yields real eigenvalues $l_{2o}/k_o = -0.372 < 0$ and $l_{3o}/k_o = -0.703 < 0$, representing an asymptotically stable (non-oscillatory) solution, or stable sink in the phase plane. Indeed, based on the condition in Eq. (137), stable non-oscillatory responses were obtained for $K_\sigma = 2K_\tau > 1.67$.

Note the apparently low influence of neglected higher order terms in Eq. (128), especially for $K_\sigma = 0.2445$, which remains neutrally stable, even for a moderate perturbation as the one introduced herein. Additional information regarding the evolution of $\mathbf{y}\,(s)$ after removing the perturbation can be extracted from the eigenvalues computed from the linearized problem, as rates of amplitude decay / grow (from their real part) or periods of oscillatory responses (from their imaginary part). For example, for $K_\sigma = 0.2445$, $\mathrm{Im}(l_{2o}) = I_o k_o = 0.0189$ days^{-1}, which yields an oscillatory period of $2\pi/\,\mathrm{Im}(l_{2o}) \approx 332$ days, consistent with the corresponding undamped response in Figure 4 computed using the associated integral-based formulation.

Lastly, it can be shown that the same qualitative behavior is obtained for mean circumferential and axial stresses for the different cases analyzed. For illustration, we show in Figure 5 the dynamic evolution of σ_θ and σ_z for $K_\sigma = 0.12$ (first row, unstable) and $K_\sigma = 0.3$ (second row, asymptotically stable). Hence, intramural stresses may eventually become unbounded for dynamically unstable situations, whereas they remained bounded in the statically unstable cases simulated above, recall Figure 3. This fact highlights the importance of identifying what kind of instability develops in an arterial wall, if any.

3.2.2. Rate parameter k_o

We comment here on the effect of the degradation rate parameter $k_o \equiv k_o^m = k_o^c > 0$ on mechanobiological stability. First, because this parameter is absent from Eqs. (110)-(112), different values of k_o do not affect the mechanobiologically equilibrated solutions given by Eq. (114); they merely influence when equilibration occurs. In case $k_o^m \neq k_o^c$, different ratios k_o^m/k_o^c yield different evolved homeostatic solutions, in general (Latorre and Humphrey 2018b). In the present case, with $k_o^m/k_o^c = k_o/k_o = 1$, different values of k_o yet

affect the dynamics of the problem. Based on the eigenvalues in Eqs. (129)-(131), or the original differential Eqs. (107)-(109), k_o defines the time scale on which the system evolves but, because the signs of (the real part of) the eigenvalues l_{io}, $i = 1, 2, 3$, remain unchanged for different $k_o > 0$, there is no change in the mechanobiological stability character of the perturbed solutions. Albeit not shown, this was confirmed numerically using our integral-based constrained mixture model with various values k_o; if the dynamic response after a transient perturbation was asymptotically stable originally (e.g., fourth row in Figure 4), an increase in k_o made the response more stable, whereas if it was unstable originally (e.g., second row in Figure 4), an increase in k_o made the response more unstable.

Substitution of Eq. (94) in Eq. (107) yields

$$\dot{\rho}_R = \dot{\rho}_R^+ - \dot{\rho}_R^- = kK_\sigma \left(\rho_R - \rho_o^e\right) \left(\Delta\sigma - (K_\tau/K_\sigma)\Delta\tau_w\right) \tag{140}$$

which means that the net production of material (i.e., difference between total production $\dot{\rho}_R^+$ and total removal $\dot{\rho}_R^-$) is proportional to kK_σ (cf., Cyron and Humphrey 2014 and Wu and Shadden 2016, wherein shear stress effects are not considered and rate and gain parameters are combined into single non-dimensionless "gain" or "growth feedback" constants). Considering a reference case I and a case II with possible different production and removal rates, with $K_\tau/K_\sigma = const$, an increased production rate with a constant removal rate (i.e., $k^{II} = k^I$) requires $K_\sigma^{II} > K_\sigma^I$ in our formulation, such that the net production $\dot{\rho}_R^{II} > \dot{\rho}_R^I$ (for equal remaining variables). However, an increased removal rate (i.e., $k^{II} > k^I$) for a constant production rate requires $K_\sigma^{II} < (k^I/k^{II})K_\sigma^I < K_\sigma^I$, such that the net production $\dot{\rho}_R^{II} < \dot{\rho}_R^I$. Hence, because changes in k_o do not modify the stability character of the system, while lower values of K_σ tend to destabilize it, we conclude that increased removal rates for preserved production rates (i.e., $k^{II} > k^I$ and $K_\sigma^{II} < (k^I/k^{II})K_\sigma^I$) tend to destabilize the system from a dynamic standpoint.

3.2.3. Material-to-prestress stiffness ratio $c_{\theta\theta}/(2\sigma_\theta)$

Similarly to k_o, the equilibrium components of the total material stiffness $\mathbb{c}(s)$ (cf. Eq. (29) for different constituents α) are absent from Eqs. (110)-(112), hence equilibrated stresses, rather than equilibrated values of stiffness, affect the mechanobiologically equili-

brated solutions given by Eq. (114). Again based on Eqs. (132) and (133), however, the circumferential equilibrium stiffness $c_{\theta\theta o}$ may modify the dynamic stability character of perturbed solutions near the original homeostatic state. In particular, the material-to-prestress stiffness ratio $c_{\theta\theta o}/(2\sigma^{ne}_{\theta o}) = c_{\theta\theta o}/(2\sigma_{\theta o} - 2\sigma^{e}_{\theta o})$ appears in both T_o and D_o. Even though the prestress $\sigma^{ne}_{\theta o} = \sigma_{\theta o} - \sigma^{e}_{\theta o}$ only accounts for the stress of constituents that turnover, namely collagen and smooth muscle cells, we analyze in this example the effect on dynamic stability of the (total) material-to-prestress stiffness ratio $c_{\theta\theta o}/(2\sigma_{\theta o})$.

The center row of panels in Figure 4 showed a neutrally stable response around the original equilibrium state that follows a 20-day impulse-like perturbation in inner pressure. For that case, $K_\sigma = 2K_\tau = 0.2445$ and, from parameters in Table 1, $c_{\theta\theta o}/(2\sigma_{\theta o}) \approx 2.5$, which yielded $R_o = \mathrm{Re}(l_{2o})/k_o = 0$ and $I_o = \mathrm{Im}(l_{2o})/k_o = 0.189$. We show in Figure 6 results computed with the same set of parameters except for the constants c^c_1 and c^c_2 for collagen, which were modified such that $\sigma_{\theta o}$ remains constant while $c_{\theta\theta o}/(2\sigma_{\theta o})$ decreases to ≈ 1.5 (first row) or increases to ≈ 3.5 (second row). Clearly, a reduction in circumferential stiffness, for constant circumferential stress, which yielded $R_o > 0$, destabilizes the referential (neutral) stable response, whereas an increase in $c_{\theta\theta o}/(2\sigma_{\theta o})$, which yielded $R_o < 0$, stabilizes it asymptotically.

Lastly, the condition in Eq. (137) predicts that the ratio $c_{\theta\theta o}/(2\sigma_{\theta o})$ should reach ≈ 29 (or higher) to yield a convergent non-oscillatory response if the gain parameters remain as low as $K_\sigma = 2K_\tau = 0.2445$. However, a more realistic, actually attainable, minimum value for stable non-oscillatory evolutions $c_{\theta\theta o}/(2\sigma_{\theta o}) \approx 5$ is predicted if the likely more physiological (cf. Section 3.2.1) values $K_\sigma = 2K_\tau = 1$ are considered. Changes in intrinsic material stiffness appear to be fundamental in thoracic aortic aneurysms (Bellini et al. 2017), hence the importance of such considerations.

3.2.4. Active contraction of muscle

The prior results have focused on the passive response of an idealized arterial wall. We analyze in this example the influence on mechanobiological stability of the active contribution to stress and stiffness given in Eqs. (64) and (69), along with (65). The first row of panels in Figure 7 show an asymptotically unstable (oscillatory) response near an associated original

homeostatic state computed with parameters in Table 1, except with $K_\sigma = 2K_\tau = 0.12$ (cf. second row in Figure 4) and an additional active contribution to stress given by $\hat{S} = 40\,\text{kPa}$, $C_B = 0.8326$, and $C_S = 0.5C_B$. The associated Jacobian matrix is such that $T_o = 0.068 > 0$ and $D_o = 0.020 > 0$, with complex eigenvalues l_{2o} and l_{3o} given by $R_o = 0.034 > 0$ and $I_o = 0.137$.

We analyze three different modifications of the active response given by the different parameters $\hat{S}$, C_B, and C_S. A fold increase in the second Piola-Kirchhoff stress-like active tone $\hat{S}$ yields the same fold increase in both equilibrated active stress, which from Eq. (64), with $\lambda_{\theta o} = 1$, $\Delta\tau_w|_o = 0$, and $C_o = C_B$, reads

$$\sigma^{act}_{\theta o} = \phi^m_o \hat{S}(1 - e^{-C_B^2}) \ , \tag{141}$$

and equilibrated active-like stiffness, which from Eq. (69), with $\tau_{wo}/\tau_{wo} = 1$ and $d\hat{S}^{act}_\theta/dC|_o = 2\hat{S}C_B e^{-C_B^2}$, reads

$$c^{act}_{\theta\theta o} = 6\phi^m_o \hat{S} C_S C_B e^{-C_B^2} \ . \tag{142}$$

A fold increase in the basal ratio C_B yields a nonlinear increase in stress, which saturates for high increments of C_B

$$\sigma^{act}_{\theta o} \to \phi^m_o \hat{S} > 0 \quad \text{for} \quad C_B \uparrow \ , \tag{143}$$

and a nonlinear decrease in stiffness, which tends to vanish

$$c^{act}_{\theta\theta o} \to 0^+ \quad \text{for} \quad C_B \uparrow \ . \tag{144}$$

Finally, a fold increase in the vasoactive parameter C_S yields no change in stress $\sigma^{act}_{\theta o}$, but the same fold change in stiffness $c^{act}_{\theta\theta o}$.

According to Eqs. (132) and (133), along with Eqs. (135) and (136), different effects on $\sigma^{act}_{\theta o}$ and $c^{act}_{\theta\theta o}$, and hence on the combined stiffness $\mathcal{C}^{act}_{\theta\theta o} = 2\sigma^{act}_{\theta o} + c^{act}_{\theta\theta o}$, lead to different dynamic responses for a given initial perturbation. We show in Figure 7, second to fourth rows, computed dynamic responses for respective 10-fold increases in $\hat{S}$, C_B, and C_S with respect to the reference case (first row). Interestingly, higher values of $\hat{S}$ (second row), which increase $\sigma^{act}_{\theta o}$ and $c^{act}_{\theta\theta o}$ proportionally, and C_S (fourth row), which increase $c^{act}_{\theta\theta o}$, stabilize

($R_o = -0.042$ and $R_o = -0.027$, respectively) the reference response ($R_o = 0.034$), whereas an equal fold increase in C_B (third row), with associated saturated stress $\sigma_{\theta o}^{act}$ and vanishing stiffness $c_{\theta\theta o}^{act}$, yields a slightly more unstable response ($R_o = 0.040$) than the referential one. Albeit not shown, intramural stresses for each case followed respective stable (second, fourth rows) or unstable (first, third rows) dynamic evolutions. Lastly, among the many possible combinations for these parameters, Eq. (137) predicts stable non-oscillatory G&R responses for a combined 7.07- or higher-fold change in both $\hat{S}$ and C_S, with C_B unchanged. The importance of active stress generation has long been known in general arterial G&R (Valentín et al. 2009) and recently was revealed in aortic dissection (Ferruzzi et al. 2016).

4. Discussion

Years ago, Waxman (1981) considered axial (buckling) instabilities in arteries as a function of prior biological growth. Although inappropriately based on linear elasticity, this paper highlighted the need to study growth and related issues of stability within a framework of continuum mechanics. Soon thereafter, Skalak et al. (1982) emphasized the need to study growth in terms of finite displacements, that is, nonlinear continuum mechanics. They also noted the possibility of unstable growth if one does not consider appropriate interdependencies in rates of allometric growth of individual structural elements. No formal stability analysis was offered, however. Somewhat surprisingly, growth mechanics did not advance much further until mid-1990s, with the introduction of a theory of finite kinematic growth. Among others who adopted this approach, Taber (1998) suggested that evolution laws for arterial adaptations to altered hemodynamics must include negative feedback, in terms of homeostatic target values, to yield stable responses. Further increasing interest in modeling G&R was the introduction of a constrained mixture approach that enabled one to consider different rates of turnover of different constituents (Humphrey and Rajagopal 2002).

There now exist many different models of soft tissue G&R based on mixture theory. For example, Klisch et al. (2003) used a mixture model to describe independent contributions of proteoglycans and collagen to the growth of cartilage. Lemon et al. (2006) used a porous flow mixture theory to study growth of engineered tissues ex vivo. Cristini et al. (2009) used a multi-phase mixture model to study the growth of avascular solid tumors. Narayanan et al.

(2009) presented a general mixture-based model of growth that coupled mass transport and tissue mechanics. Haider et al. (2011) used a mixture model to study matrix production in a cell-seeded tissue engineered scaffold for cartilage. Cowin and Cardoso (2012) proposed a general mixture-based poroelastic model of interstitial growth. Ateshian et al. (2014) modeled interstitial tissue growth by considering both the solid mechanics and biochemical reactions. Soares and Sacks (2016) used a triphasic constrained mixture model to describe engineered tissue formation under in vitro dynamic mechanical loading. Vernerey (2016) used a constrained mixture model of interstitial growth in polymeric scaffolds for tissue engineering. Truster and Masud (2017) similarly used a mixture theory to study the infiltration of cells and neotissue formation within degrading polymeric scaffolds used for tissue engineering. Additional discussion of these and other mixture approaches can be found in Ambrosi et al. (2011) and Ateshian and Humphrey (2012). Note, too, that Watton et al. (2004) and Baek et al. (2006) used mixture-based computational models to study aneurysmal G&R. Whereas the former reported an unstable / unbounded enlargement of these lesions, the latter showed that multiple parameters (e.g., rates of tissue production and preferential alignment of the new tissue) can stabilize the enlargement, at least when production rates depend on differences in stress from homeostatic targets, consistent with the suggestion of Taber (1998). Again, however, these works did not consider formal stability analyses. In contrast, Ben Amar and Goriely (2005) noted that growth can alter both the geometry of and residual stress field within a tissue, each of which can affect mechanical stability under near static loading. Specifically, these authors contrasted cases wherein prior growth could either stabilize (via wall thickening or tensile residual stresses) or destabilize (via thinning or compressive residual stresses) a prototypical thick-walled, neoHookean spherical shell model of a tissue. Revisiting the study of Waxman (1981), Goriely and Vandiver (2010) used similar ideas to study axial buckling of arteries subjected to increasing pressures.

More recent studies have instead focused on the stability of the G&R process itself (i.e., mechanobiological stability) rather than the mechanical stability that results from prior G&R. Erlich et al. (2019) studied the possible stability of the growth of layered tubular structures that exhibit an isotropic, materially uniform behavior; they used the concept of kinematic growth rather than a mixture approach. Additionally, Satha et al. (2014), Cyron

et al. (2014), and Wu and Shadden (2016) used different approaches to study the stability of G&R in arteries and arrived at consistent conclusions. Increased tissue stiffness and higher rates of tissue production tend to stabilize G&R processes under constant pressures while increased rates of degradation can destabilize the G&R. Hence, there is an acute need to consider parameter values carefully, both to identify optimal G&R capacity and to determine whether a process will or will not be mechanobiologically stable.

In this paper, we sought both to develop a general framework and to illustrate consequences of G&R stabilities by performing a systematic, formal analysis for idealized arteries while yet accounting for complexities such as different nonlinear material properties and rates of turnover for different structurally significant constituents and including intramural biaxial and wall shear stresses as stimuli for mass production as well as active and passive contributions of smooth muscle. Toward this end, we first derived a new rate-based form for a constrained mixture that is equivalent to the traditional heredity integral-based form but facilitates linearized stability analyses about appropriate mechanobiological equilibria. Numerical simulations confirmed this equivalency, at least for the canonical problems considered. This rate-form revealed, among other findings, the appropriateness of the Truesdell stress rate in constrained mixture G&R formulations and the natural separation of rates of change of stress into elastic and inelastic parts, the latter in terms of "growth" and "remodeling" aspects. We next derived a system of nonlinear ordinary differential equations for G&R of a cylindrical artery that admitted both an analysis of critical points and an eigenvalue analysis of respective linearized systems. The former led to the concept of mechanobiological *static* stability of mechanobiologically equilibrated states, which allows one to analyze how soft tissues adapt to sustained changes in external loads or material properties, with G&R time s conveniently eliminated from the analysis; the latter led to the concept of mechanobiological *dynamic* stability of perturbed solutions around previously equilibrated states. For the arterial model considered, these analyses delineated two different types of possible instabilities, namely, asymptotic growth of static equilibria and asymptotic growth of dynamic responses around (bounded) equilibrated states.

Regarding the novel concept of mechanobiological static stability of G&R states, our findings are consistent with prior studies that showed a destabilizing effect of elastin degra-

dation (cf. Watton et al. 2004, Zeinali-Davarani et al. 2011, and Valentín et al. 2013). Yet, even though this G&R problem in the aorta, leading to aneurysm growth, is frequently addressed from a time-dependent perspective, we confirmed that its ultimate cause may be a mechanobiological instability of the evolving equilibrium state (Cyron et al. 2014), which we directly addressed with a static approach. Analyses of this type driven by other external loads or material parameters could lead to other types of static instabilities, such as limit points or bifurcations.

Additional findings related to the mechanobiological stability of transiently perturbed evolutions around equilibrium states were consistent with other studies that showed the stabilizing effects of increased material stiffness and tissue production rates and destabilizing effects of increased removal rates (cf. Satha et al. 2014, Cyron et al. 2014, and Wu and Shadden 2016). At least for the constitutive relations and model parameters used, we additionally showed that gain parameters for mass production that are associated with both intramural biaxial and wall shear stresses play important roles in the eigenvalue analysis and that an increasing active contribution to stress was stabilizing. Consistent with the type and sign of the eigenvalues of the Jacobian matrix, determined analytically for the original homeostatic state, numerical simulations further revealed that unstable, neutrally stable, or asymptotically stable results could arise mathematically in response to transient perturbations depending on specific model assumptions or values of the parameters, hence extending the analysis of Satha et al. (2014). In this regard, note that we focused on the stability of an idealized and isolated growing artery from a constitutive point of view, disregarding other factors that could damp oscillations, including external perivascular support or additional intrinsic dissipation. Nevertheless, as we illustrated in examples above, mathematical analyses of this type can serve to identify conditions that ensure a physiologically reasonable dynamics predicted by the G&R constitutive model.

Our theory, based originally on fully coupled nonlinear evolutions of mass and stress (Fung 1995), thus builds on the mechanobiological stability theory of Cyron and Humphrey (2014), where mechanical stability (against displacement perturbations) and mechanobiological stability (against mass perturbations) were analyzed incrementally based on a theory of small on large (Baek et al. 2007a) extended to G&R by distinguishing elastic and inelastic

deformations. Mechanobiologically stable systems considered therein, with sustained and transient responses analyzed together, were always neutrally (Lyapunov) stable under small, residual perturbations with respect to the original state, leading to associated definitions of mechanobiological adaptivities. Using a linearized stress-strain relation with respect to a homeostatic state of the vessel wall, among other assumptions, Wu and Shadden (2016) also found a neutrally stabilizing condition, or degeneration, when the dynamics of displacement and mass variables were decoupled from the dynamics of an additional generalized stiffness variable. Further use of an extended system led to the main stability conclusions that displacements and mass were neutrally stable whereas stress and stiffness were asymptotically stable. In contrast, our formulation, based on nonlinear constitutive relations for multiple constituents that may turnover or not, did not lead, by default, to a degenerate system of this kind; rather, neutral stability in the sense of Lyapunov around evolved critical points was obtained only for particular cases. In general, mechanobiological dynamic stability following the nonlinear equations considered herein exhibited an asymptotic character, either oscillatory or not, under moderate perturbations. Because of the lack of empirical evidence of oscillatory behaviors in vivo, these findings can aid further in refining values of parameters that are physiologically meaningful and yet revealing.

In conclusion, it is becoming increasingly evident that mechanical homeostasis is fundamental to healthy tissue structure and function and conversely that compromised or lost homeostasis underlies many cases of disease (Humphrey et al. 2014). Homeostasis necessarily implies negative feedback loops that govern G&R processes at the tissue level, with target values of appropriate mechanical metrics. It has recently been suggested that the converse, that is positive feedback loops, implies disease progression, leading to a type of biological instability (Schwartz et al. 2018). We suggest that mechanobiological stability analyses, such as those performed herein, promise to provide increasing insight into general processes that promote health versus disease progression. There is, therefore, a pressing need to continue to broaden and advance our constitutive relations for G&R, building on new biological findings as they become available while continuing to capture fundamental features of soft tissues, including the different material properties, rates of turnover, and natural configurations of the different structural constituents.

Acknowledgments

This work was supported, in part, by grants from the US NIH, namely, R01 HL105297 (to C.A. Figueroa and J.D. Humphrey), R01 HL128602 (to J.D. Humphrey, C.K. Breuer, and Y. Wang), P01 HL134605 (to G. Tellides and J.D. Humphrey via a PPG to D. Rifkin), and U01 HL142518 (to J.D. Humphrey and G.E. Karniadakis).

Conflict of Interest

The authors declare that they have no conflict of interest.

Artery Mass Density	ρ	$1050\,\mathrm{kg/m^3}$
Inner Radius, Wall Thickness	a_o, h_o	$[0.6468, 0.0402]\,\mathrm{mm}$
Mass Fractions	$\phi_o^e, \phi_o^m, \phi_o^c$	$[0.30, 0.35, 0.35]$
Collagen Fractions	$\beta^\theta, \beta^z, \beta^d$	$[0.068, 0.381, 0.551]$
Diagonal Collagen Orientation	α_0	45.36^o
Elastin Parameter	c^e	$114.5\,\mathrm{kPa}$
Smooth Muscle Parameters	c_1^m, c_2^m	$[401.0\,\mathrm{kPa}, 0.012]$
Collagen Parameters	c_1^c, c_2^c	$[411.2\,\mathrm{kPa}, 5.5]$
Deposition Stretches	G_r^e, G_θ^e, G_z^e	$[1/(1.9 \cdot 1.6), 1.9, 1.6]$
Deposition Stretches	$G_\theta^m = G_\theta^c, G_z^c, G_d^c$	$[1.071, 1.193, 1.192]$
Mass Production Gains	K_σ, K_τ	$[1.0, 0.5]$
Mass Removal Rate	k_o	$1/10\ \mathrm{day}^{-1}$

Table 1: Representative baseline model parameters for a mouse descending thoracic aorta, adapted (homogenized through the thickness) from Latorre and Humphrey (2018a). Superscripts e, m, c denote elastin, smooth muscle, and collagen, with superscripts/subscripts r, θ, z, d denoting radial, circumferential, axial, and symmetric diagonal directions. Subscript o denotes original homeostatic values. Subscripts σ and τ denote intramural and wall shear stress related parameters, respectively.

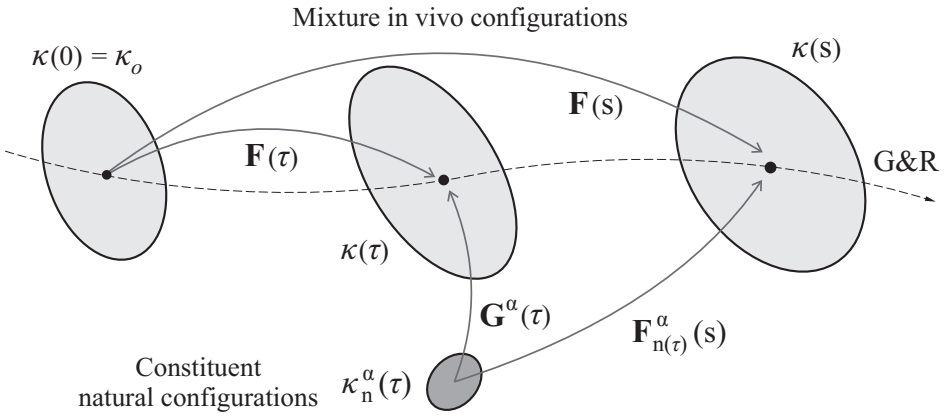

Figure 1: Schematic representation of different configurations involved in soft tissue G&R. The original in vivo homeostatic configuration of the mixture $\kappa(0) = \kappa_o$ is chosen as the reference configuration for the computation of G&R deformations of the mixture via $\mathbf{F}(\tau)$, $\tau \in [0, s]$. $\mathbf{F}^\alpha_{n(\tau)}(s) = \mathbf{F}(s)\,\mathbf{F}^{-1}(\tau)\,\mathbf{G}^\alpha(\tau)$ describes the deformation experienced, at time s, by the material element of constituent α deposited at time τ. We assume that the constituents, deposited with prestretches $\mathbf{G}^\alpha(\tau)$, are constrained to deform with the mixture.

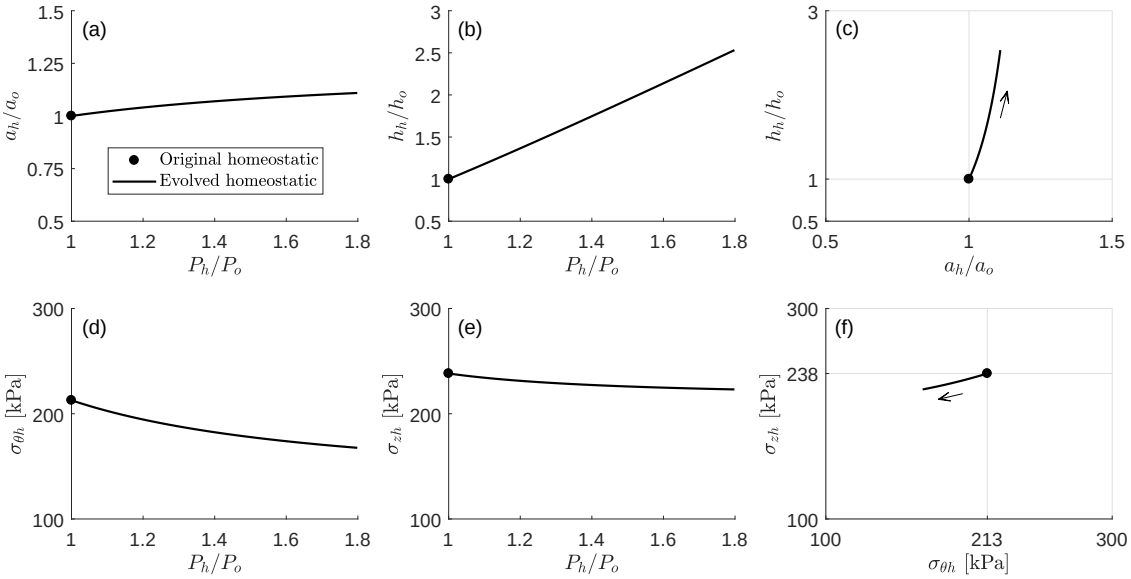

Figure 2: Mechanobiologically stable (static) equilibrium responses illustrated for a "normal" murine aorta. Panels (a,b,d,e) show equilibrium values for (bounded) inner radius a_h and thickness h_h, as well as (bounded) circumferential $\sigma_{\theta h}$ and axial σ_{zh} Cauchy stress, as functions of the stimulation-driver pressure ratio $\gamma_h = P_h/P_o$. Panels (c) and (f) show the associated evolution of the homeostatic state in phase-type planes: thickening with slight dilation and slight reduction in biaxial stress. Note, too, that the thickening is not fully mechano-adaptive, consistent with experimental observations for the murine thoracic aorta (Bersi et al. 2016).

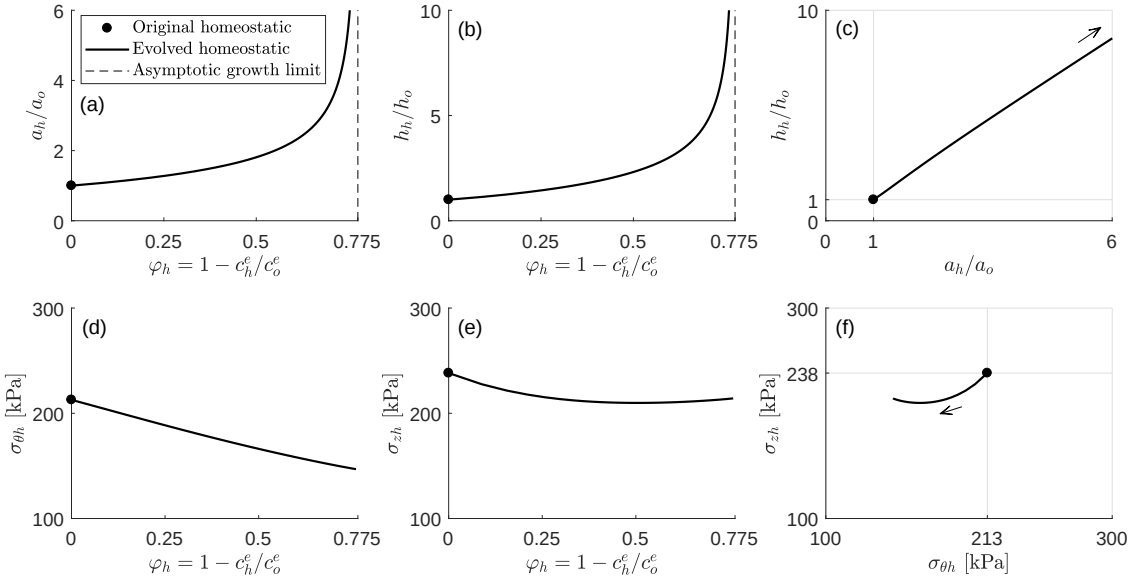

Figure 3: Mechanobiologically unstable (static) equilibrium responses with respect to prior elastin degradation while preserving inner pressure $P_h = P_o$. Panels (a,b,d,e) show equilibrium values for (unbounded) inner radius a_h and thickness h_h, as well as (bounded) circumferential $\sigma_{\theta h}$ and axial σ_{zh} Cauchy stress, as functions of the stimulation-driver parameter $\varphi_h = (c_o^e - c_h^e)/c_o^e$. Panels (c) and (f) show the associated evolution of the homeostatic state in phase-type planes: asymptotic thickening and dilation with moderate reduction in biaxial stress.

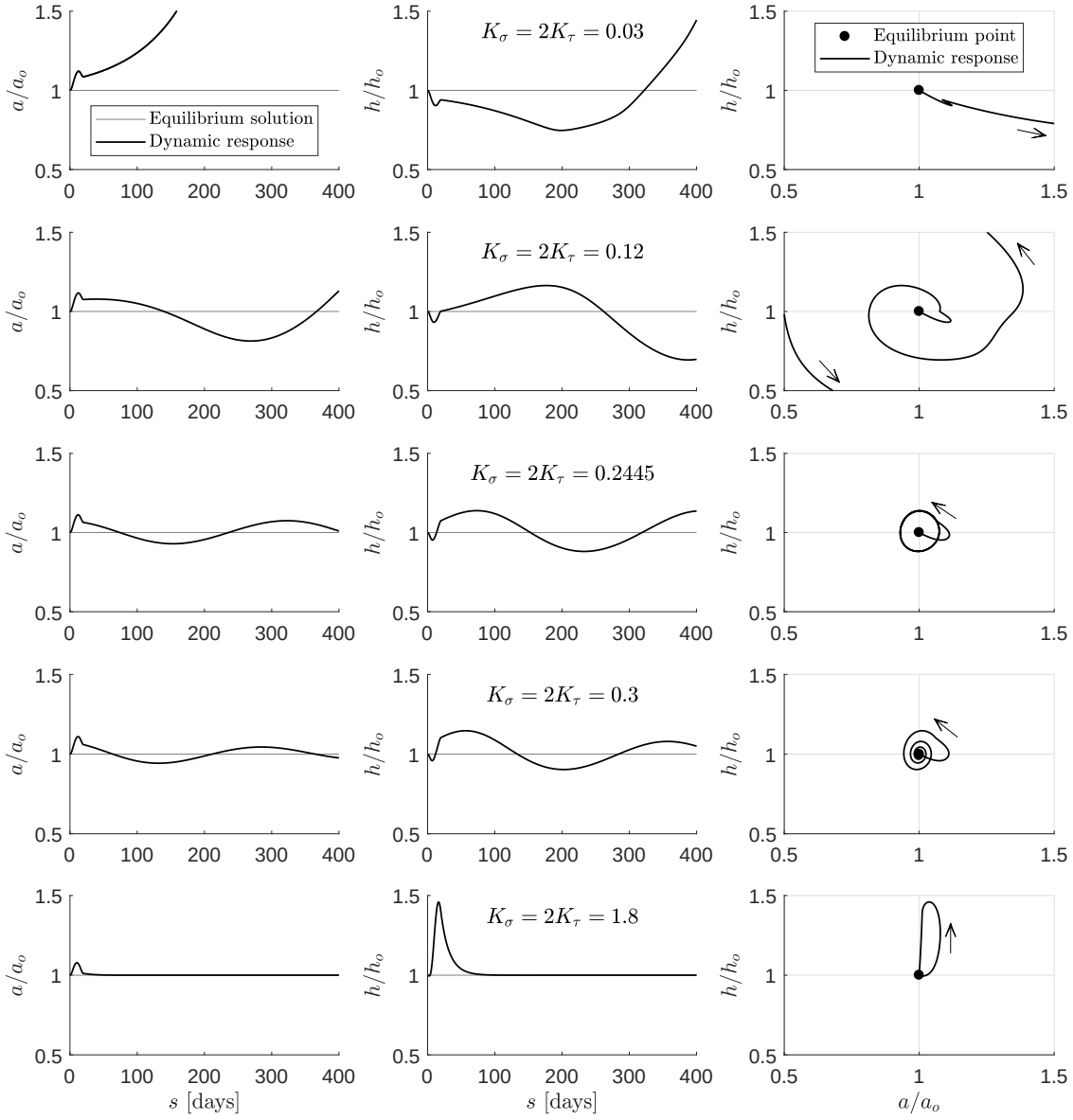

Figure 4: Mechanobiologically unstable ($K_\sigma = 0.03$, "source", and $K_\sigma = 0.12$, "spiral"; top two rows), neutral stable ($K_\sigma = 0.2445$, "center"; third row), and asymptotic stable ($K_\sigma = 0.3$, "spiral", and $K_\sigma = 1.8$, "sink"; bottom two rows) dynamic responses that follow a perturbation in pressure, consisting of a rapid rise from P_o up to $1.5P_o$ at $s = 0^+$ days, subsequently sustained for 20 days, and finally returned back to the original homeostatic value P_o at $s = 20^+$ days. For all cases, $K_\tau = K_\sigma/2$.

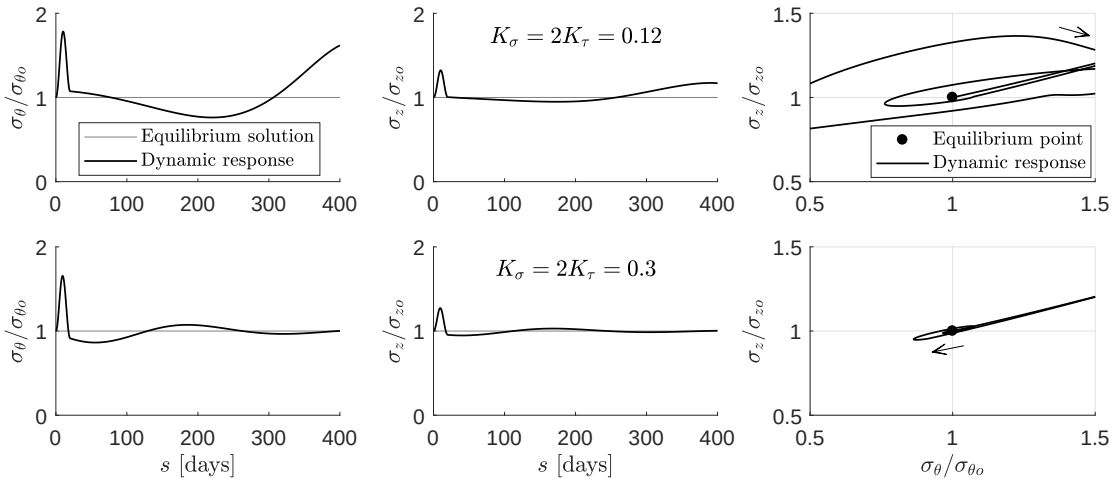

Figure 5: Dynamic stress response (σ_θ and σ_z) for cases $K_\sigma = 0.12$ (cf. unstable spiral; second row, Fig. 4) and $K_\sigma = 0.3$ (cf. stable spiral; fourth row, Fig. 4).

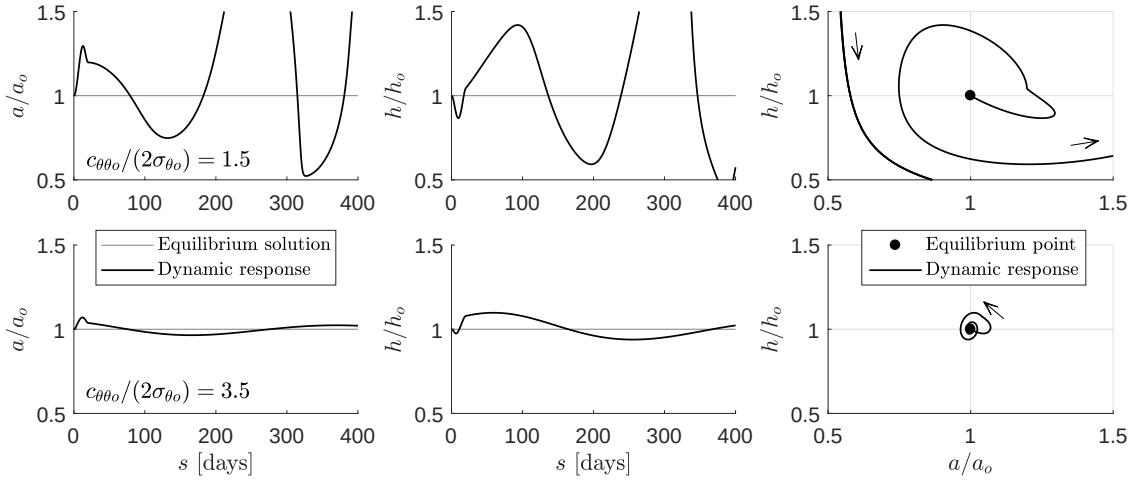

Figure 6: Dynamic stabilization afforded by an increased ratio of circumferential stiffness to material prestress $c_{\theta\theta o}/(2\sigma_{\theta o})$. Panels in first row show an unstable oscillatory response with $K_\sigma = 2K_\tau = 0.2445$ and $c_{\theta\theta o}/(2\sigma_{\theta o}) \approx 1.5$ (cf. third row, Fig. 4, wherein $K_\sigma = 2K_\tau = 0.2445$ and $c_{\theta\theta o}/(2\sigma_{\theta o}) \approx 2.5$). Panels in second row show results for $c_{\theta\theta o}/(2\sigma_{\theta o}) \approx 3.5$, which stabilizes asymptotically the prior neutrally stable response.

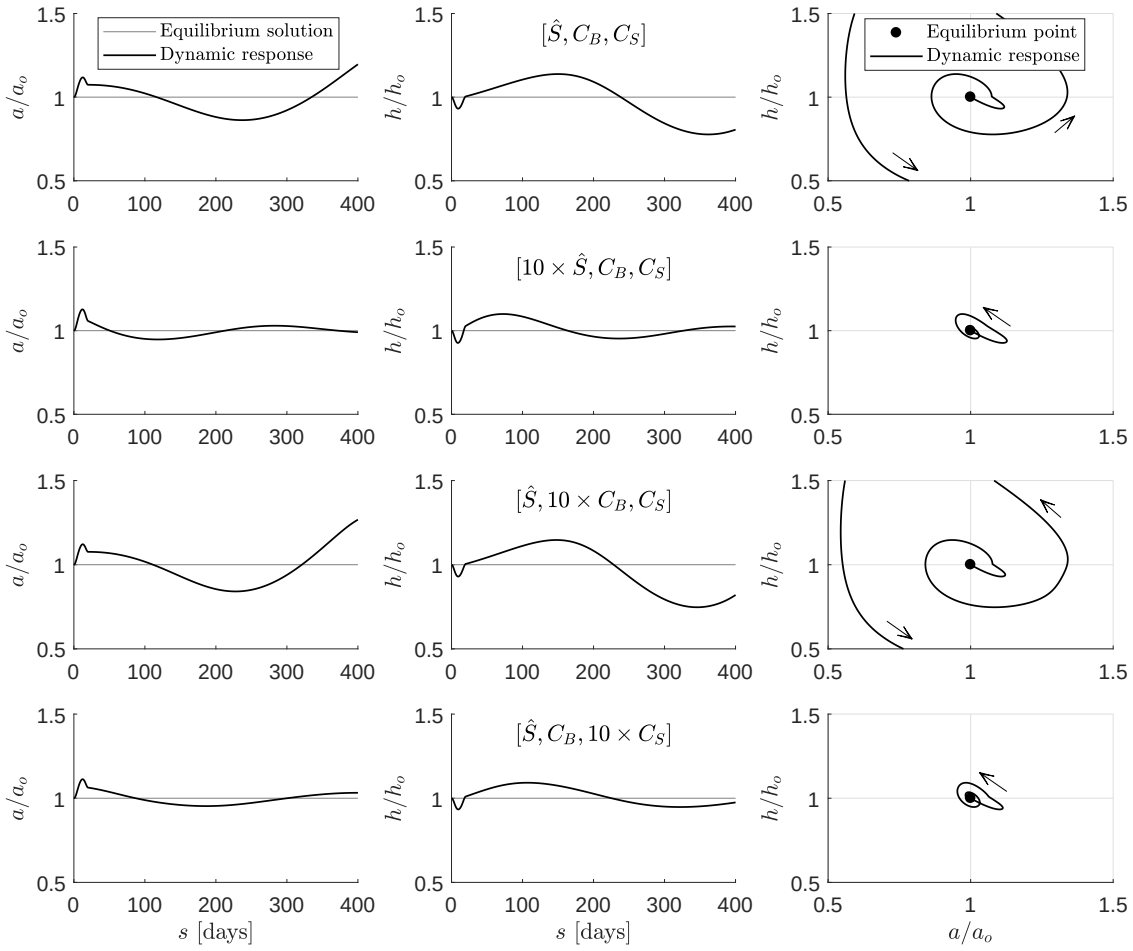

Figure 7: Dynamic stabilization by the active response of smooth muscle cells. Panels in first row show an unstable response with passive (Table 1, except for $K_\sigma = 2K_\tau = 0.12$; cf. second row, Fig. 4) and additional active ($\hat{S} = 40\,\text{kPa}$, $C_B = 0.8326$, $C_S = 0.5C_B$) contributions to stress. A 10-fold increase in either $\hat{S}$ (second row) or C_S (fourth row) stabilize the prior response (first row). A 10-fold increase in C_B (third row) has little effect over the prior response, even augmenting the instability.

References

Ambrosi D, Ateshian GA, Arruda EM, Cowin SC, Dumais J, Goriely A, Holzapfel GA, Humphrey JD, Kemkemer R, Kuhl E, Olberding JE, Taber LA, Garikipati K (2011) Perspectives on biological growth and remodeling. Journal of the Mechanics and Physics of Solids 59(4):863–883

Ateshian GA, Humphrey JD (2012) Continuum mixture models of biological growth and remodeling: past successes and future opportunities. Annual review of biomedical engineering 14:97–111

Ateshian GA, Nims RJ, Maas S, Weiss JA (2014) Computational modeling of chemical reactions and interstitial growth and remodeling involving charged solutes and solid-bound molecules. Biomechanics and modeling in mechanobiology 13(5):1105–1120

Baek S, Rajagopal KR, Humphrey JD (2006) A theoretical model of enlarging intracranial fusiform aneurysms. Journal of biomechanical engineering 128(1):142–149

Baek S, Gleason RL, Rajagopal KR, Humphrey JD (2007a) Theory of small on large: potential utility in computations of fluid–solid interactions in arteries. Computer Methods in Applied Mechanics and Engineering 196(31-32):3070–3078

Baek S, Valentín A, Humphrey JD (2007b) Biochemomechanics of cerebral vasospasm and its resolution: II. constitutive relations and model simulations. Annals of Biomedical Engineering 35(9):1498–1509

Bellini C, Ferruzzi J, Roccabianca S, Di Martino ES, Humphrey JD (2014) A microstructurally motivated model of arterial wall mechanics with mechanobiological implications. Annals of Biomedical Engineering 42(3):488–502

Bellini C, Bersi MR, Caulk AW, Ferruzzi J, Milewicz DM, Ramirez F, Rifkin DB, Tellides G, Yanagisawa H, Humphrey JD (2017) Comparison of 10 murine models reveals a distinct biomechanical phenotype in thoracic aortic aneurysms. Journal of The Royal Society Interface 14(130):20161036

Ben Amar M, Goriely A (2005) Growth and instability in elastic tissues. Journal of the Mechanics and Physics of Solids 53(10):2284–2319

Bersi MR, Bellini C, Wu J, Montaniel KRC, Harrison DG, Humphrey JD (2016) Excessive adventitial remodeling leads to early aortic maladaptation in angiotensin-induced hypertension. Hypertension 67:890–896

Boyce WE, DiPrima RC (2012) Elementary differential equations and boundary value problems, 10th edn. JohnWiley & Sons, New Jersey

Cowin SC, Cardoso L (2012) Mixture theory-based poroelasticity as a model of interstitial tissue growth. Mechanics of Materials 44:47–57

Cristini V, Li X, Lowengrub JS, Wise SM (2009) Nonlinear simulations of solid tumor growth using a mixture model: invasion and branching. Journal of mathematical biology 58(4-5):723

Cyron CJ, Humphrey JD (2014) Vascular homeostasis and the concept of mechanobiological stability. International journal of engineering science 85:203–223

Cyron CJ, Wilson JS, Humphrey JD (2014) Mechanobiological stability: a new paradigm to understand the enlargement of aneurysms? Journal of the Royal Society Interface 11(100):20140680

Cyron CJ, Aydin RC, Humphrey JD (2016) A homogenized constrained mixture (and mechanical analog) model for growth and remodeling of soft tissue. Biomechanics and Modeling in Mechanobiology 15(6):1389–1403

Erlich A, Moulton DE, Goriely A (2019) Are homeostatic states stable? Dynamical stability in morphoelasticity. Bulletin of Mathematical Biology 81(8):3219–3244

Ferruzzi J, Murtada SI, Li G, Jiao Y, Uman S, Ting MYL, Tellides G, Humphrey JD (2016) Pharmacologically improved contractility protects against aortic dissection in mice with disrupted transforming growth factor-β signaling despite compromised extracellular matrix properties. Arteriosclerosis, thrombosis, and vascular biology 36:919–927

Fung YC (1995) Stress, strain, growth, and remodeling of living organisms. In: Casey J, Crochet MJ (eds) Theoretical, Experimental, and Numerical Contributions to the Mechanics of Fluids and Solids, Birkhäuser, Basel, pp 469–482

Gleason RL, Wilson E, Humphrey JD (2007) Biaxial biomechanical adaptations of mouse carotid arteries cultured at altered axial extension. Journal of biomechanics 40(4):766–776

Goriely A, Vandiver R (2010) On the mechanical stability of growing arteries. IMA journal of applied mathematics 75(4):549–570

Haider MA, Olander JE, Arnold RF, Marous DR, McLamb AJ, Thompson KC, Woodruff WR, Haugh JM (2011) A phenomenological mixture model for biosynthesis and linking of cartilage extracellular matrix in scaffolds seeded with chondrocytes. Biomechanics and modeling in mechanobiology 10(6):915–924

Hairer E, Nørsett SP, Wanner G (1993) Solving Ordinary Differential Equations: I. Nonstiff Problems, 2nd edn. Series in Computational Mathematics (8), Springer Verlag

Haslach HW, Humphrey JD (2004) Dynamics of biological soft tissue and rubber: internally pressurized spherical membranes surrounded by a fluid. International Journal of Non-Linear Mechanics 39(3):399–420

Holzapfel GA (1996) On large strain viscoelasticity: continuum formulation and finite element applications to elastomeric structures. International Journal for Numerical Methods in Engineering 39(22):3903–3926

Holzapfel GA (2000) Nonlinear Solid Mechanics. A Continuum Approach for Engineering. John Wiley & Sons, Chichester

Humphrey JD (2002) Cardiovascular Solid Mechanics: Cells, Tissues and Organs. Springer-Verlag, New York

Humphrey JD, Rajagopal KR (2002) A constrained mixture model for growth and remodeling of soft tissues. Mathematical Models and Methods in Applied Sciences 12(03):407–430

Humphrey JD, Eberth JF, Dye WW, Gleason RL (2009) Fundamental role of axial stress in compensatory adaptations by arteries. Journal of biomechanics 42(1):1–8

Humphrey JD, Dufresne ER, Schwartz MA (2014) Mechanotransduction and extracellular matrix homeostasis. Nature Reviews Molecular Cell Biology 15(12):802–812

Hynes RO, Naba A (2012) Overview of the matrisome—an inventory of extracellular matrix constituents and functions. Cold Spring Harbor perspectives in biology 4(1):A004903

Klisch SM, Chen SS, Sah RL, Hoger A (2003) A growth mixture theory for cartilage with application to growth-related experiments on cartilage explants. Journal of biomechanical engineering 125(2):169–179

Latorre M, Humphrey JD (2018a) Critical roles of time-scales in soft tissue growth and remodeling. APL Bioengineering 2(2):026108

Latorre M, Humphrey JD (2018b) A mechanobiologically equilibrated constrained mixture model for growth and remodeling of soft tissues. ZAMM-Journal of Applied Mathematics and Mechanics 98:2048–2071

Latorre M, Humphrey JD (2018c) Modeling mechano-driven and immuno-mediated aortic maladaptation in hypertension. Biomechanics and Modeling in Mechanobiology 17(5):1497–1511

Latorre M, Montáns FJ (2015) Anisotropic finite strain viscoelasticity based on the Sidoroff multiplicative decomposition and logarithmic strains. Computational Mechanics 56(3):503–531

Lemon G, King JR, Byrne HM, Jensen OE, Shakesheff KM (2006) Mathematical modelling of engineered tissue growth using a multiphase porous flow mixture theory. Journal of mathematical biology 52(5):571–594

Lyapunov AM (1882) Problème général de la stabilité du mouvement. Annals of Mathematics Studies (17), Princeton University Press (Reprint 1947)

Miller KS, Lee YU, Naito Y, Breuer CK, Humphrey JD (2014) Computational model of the in vivo development of a tissue engineered vein from an implanted polymeric construct. Journal of Biomechanics 47(9):2080–2087

Murtada SI, Humphrey JD, Holzapfel GA (2017) Multiscale and multiaxial mechanics of vascular smooth muscle. Biophysical journal 113(3):714–727

Narayanan H, Arruda EM, Grosh K, Garikipati K (2009) The micromechanics of fluid–solid interactions during growth in porous soft biological tissue. Biomechanics and modeling in mechanobiology 8(3):167

Ramachandra AB, Humphrey JD, Marsden AL (2017) Gradual loading ameliorates maladaptation in computational simulations of vein graft growth and remodelling. Journal of The Royal Society Interface 14(130):20160995

Rouche N, Habets P, Laloy M (1977) Stability theory by Liapunov's direct method. Applied Mathemathical Sciences (22), Springer Verlag

Satha G, Lindström SB, Klarbring A (2014) A goal function approach to remodeling of arteries uncovers mechanisms for growth instability. Biomechanics and modeling in mechanobiology 13(6):1243–1259

Schwartz MA, Vestweber D, Simons M (2018) A unifying concept in vascular health and disease. Science 360(6386):270–271

Sidoroff F (1974) Un modèle viscoélastique non linéaire avec configuration intermédiaire. Journal de Mécanique 13(4):679–713

Simó JC (1987) On a fully three-dimensional finite-strain viscoelastic damage model: formulation and computational aspects. Computer methods in applied mechanics and engineering 60(2):153–173

Simó JC, Pister KS (1984) Remarks on rate constitutive equations for finite deformation problems: computational implications. Computer Methods in Applied Mechanics and Engineering 46(2):201–215

Skalak R, Dasgupta G, Moss M, Otten E, Dullemeijer P, Vilmann H (1982) Analytical description of growth. Journal of theoretical biology 94(3):555–577

Soares JS, Sacks MS (2016) A triphasic constrained mixture model of engineered tissue formation under in vitro dynamic mechanical conditioning. Biomechanics and modeling in mechanobiology 15(2):293–316

Taber L (1998) A model for aortic growth based on fluid shear and fiber stresses. Journal of biomechanical engineering 120(3):348–354

Truster TJ, Masud A (2017) A unified mixture formulation for density and volumetric growth of multi-constituent solids in tissue engineering. Computer Methods in Applied Mechanics and Engineering 314:222–268

Valentín A, Humphrey JD (2009) Evaluation of fundamental hypotheses underlying constrained mixture models of arterial growth and remodelling. Philosophical Transactions of the Royal Society of London A: Mathematical, Physical and Engineering Sciences 367(1902):3585–3606

Valentín A, Cardamone L, Baek S, Humphrey JD (2009) Complementary vasoactivity and matrix remodelling in arterial adaptations to altered flow and pressure. Journal of The Royal Society Interface 6(32):293–306

Valentín A, Humphrey JD, Holzapfel GA (2013) A finite element-based constrained mixture implementation for arterial growth, remodeling, and adaptation: Theory and numerical verification. International journal for numerical methods in biomedical engineering 29(8):822–849

Vernerey FJ (2016) A mixture approach to investigate interstitial growth in engineering scaffolds. Biomechanics and modeling in mechanobiology 15(2):259–278

Wagenseil JE, Mecham RP (2009) Vascular extracellular matrix and arterial mechanics. Physiological reviews 89(3):957–989

Watton PN, Hill NA, Heil M (2004) A mathematical model for the growth of the abdominal aortic aneurysm. Biomechanics and modeling in mechanobiology 3(2):98–113

Waxman AM (1981) A continuum approach to blood vessel growth: Axisymmetric elastic structures. Journal of theoretical biology 91(2):273–301

Wu J, Shadden SC (2016) Stability analysis of a continuum-based constrained mixture model for vascular growth and remodeling. Biomechanics and modeling in mechanobiology 15(6):1669–1684

Zeinali-Davarani S, Sheidaei A, Baek S (2011) A finite element model of stress-mediated vascular adaptation: application to abdominal aortic aneurysms. Computer methods in biomechanics and biomedical engineering 14(9):803–817

Appendix A. Constitutive tangent moduli

Elastin

$$c^e_{jk}(s) = \frac{\phi^e_o}{J(s)} \lambda^2_j(s)\, \lambda^2_k(s)\, G^{e2}_j G^{e2}_k \hat{C}^e_{jk}(s) \;\;, \quad j,k = \{r,\theta,z\} \tag{A.1}$$

Smooth muscle

$$c^m_{\theta\theta}(s) = \frac{\lambda^4_\theta(s)}{J(s)\,\rho} \int_{-\infty}^{s} k^m(\tau)\, \Upsilon^m(\tau)\, q^m(s,\tau)\, \frac{\rho^m_R(\tau)\, G^{m4}_\theta \hat{C}^m_{\theta\theta}(s,\tau)}{\lambda^4_\theta(\tau)} d\tau \tag{A.2}$$

Collagen

$$\begin{aligned} c^c_{\theta\theta}(s) = {} & \frac{\lambda^4_\theta(s)}{J(s)\,\rho} \int_{-\infty}^{s} k^c(\tau)\, \Upsilon^c(\tau)\, q^c(s,\tau)\, \frac{\rho^c_{R\theta}(\tau)\, G^{c4}_\theta \hat{C}^c_{\theta\theta}(s,\tau)}{\lambda^4_\theta(\tau)} d\tau \\ & + \frac{\lambda^4_\theta(s)}{J(s)\,\rho} \int_{-\infty}^{s} k^c(\tau)\, \Upsilon^c(\tau)\, q^c(s,\tau)\, \frac{\rho^c_{Rd}(\tau)\, G^{c4}_d \hat{C}^c_{dd}(s,\tau)}{\lambda^4_\theta(\tau)} \sin^4 \alpha_d d\tau \end{aligned} \tag{A.3}$$

$$\begin{aligned} c^c_{zz}(s) = {} & \frac{\lambda^4_z(s)}{J(s)\,\rho} \int_{-\infty}^{s} k^c(\tau)\, \Upsilon^c(\tau)\, q^c(s,\tau)\, \frac{\rho^c_{Rz}(\tau)\, G^{c4}_z \hat{C}^c_{zz}(s,\tau)}{\lambda^4_z(\tau)} d\tau \\ & + \frac{\lambda^4_z(s)}{J(s)\,\rho} \int_{-\infty}^{s} k^c(\tau)\, \Upsilon^c(\tau)\, q^c(s,\tau)\, \frac{\rho^c_{Rd}(\tau)\, G^{c4}_d \hat{C}^c_{dd}(s,\tau)}{\lambda^4_z(\tau)} \cos^4 \alpha_d d\tau \end{aligned} \tag{A.4}$$

$$c^c_{\theta z}(s) = \frac{\lambda^2_\theta(s)\, \lambda^2_z(s)}{J(s)\,\rho} \int_{-\infty}^{s} k^c(\tau)\, \Upsilon^c(\tau)\, q^c(s,\tau)\, \frac{\rho^c_{Rd}(\tau)\, G^{c4}_d \hat{C}^c_{dd}(s,\tau)}{\lambda^2_\theta(\tau)\, \lambda^2_z(\tau)} \sin^2 \alpha_d \cos^2 \alpha_d d\tau \tag{A.5}$$

Active contribution

$$c_{\theta\theta}^{act}(s) = 3\phi^m(s)\,\lambda_\theta^2(s)\,C_S \frac{d\hat{S}_\theta^{act}\left(C(s)\right)}{dC(s)} \frac{\tau_w(s)}{\tau_{wo}} \tag{A.6}$$

Mechanobiologically equilibrated values

$$\sigma_{\theta o} = \sum_{\alpha}^{e,m,c,act} \sigma_{\theta o}^{\alpha} = \phi_o^e \hat{S}_\theta^e G_\theta^{e2} + \phi_o^m \hat{S}_\theta^m G_\theta^{m2} + \phi_o^c \left(\beta_\theta \hat{S}_\theta^c G_\theta^{c2} + \beta_d \hat{S}_d^c G_d^{c2} \sin^2\alpha_d\right) + \sigma_{\theta o}^{act} \tag{A.7}$$

$$\sigma_{\theta o}^e = \phi_o^e \hat{\sigma}_\theta^e = \phi_o^e \hat{S}_\theta^e G_\theta^{e2}\ , \qquad \hat{\sigma}_{zo}^e = \hat{S}_z^e G_z^{e2} \tag{A.8}$$

$$\sigma_{zo} = \sum_{\alpha}^{e,c} \sigma_{zo}^{\alpha} = \sum_{\alpha}^{e,c} \phi_o^{\alpha} \hat{\sigma}_z^{\alpha} = \phi_o^e \hat{S}_z^e G_z^{e2} + \phi_o^c \left(\beta_z \hat{S}_z^c G_z^{c2} + \beta_d \hat{S}_d^c G_d^{c2} \cos^2\alpha_d\right) \tag{A.9}$$

$$\sigma_{\theta o}^{act} = \phi_o^m \hat{S}(1 - e^{-C_B^2})\ , \qquad c_{\theta\theta o}^{act} = 6\phi_o^m \hat{S} C_S C_B e^{-C_B^2} \tag{A.10}$$

$$c_{\theta\theta o} = \sum_{\alpha}^{e,m,c,act} c_{\theta\theta o}^{\alpha} = 0 + \phi_o^m \hat{C}_{\theta\theta}^m G_\theta^{m4} + \phi_o^c \left(\beta_\theta \hat{C}_{\theta\theta}^c G_\theta^{c4} + \beta_d \hat{C}_{dd}^c G_d^{c4} \sin^4\alpha_d\right) + c_{\theta\theta o}^{act} \tag{A.11}$$

$$c_{\theta z o} = \sum_{\alpha}^{e,c} c_{\theta z o}^{\alpha} = 0 + \phi_o^c \beta_d \hat{C}_{dd}^c G_d^{c4} \sin^2\alpha_d \cos^2\alpha_d = \phi_o^c \beta_d \hat{C}_{dd}^c G_d^{c4} \sin^2\alpha_d \cos^2\alpha_d \tag{A.12}$$

Appendix B. Jacobian matrix derivatives

Auxiliary results

$$\frac{\partial\left(\tau_w/\tau_{wo}\right)}{\partial\rho_R} = -\frac{3}{2}\left(\frac{\rho\sigma_{\theta o}}{\rho_R\sigma_\theta}\right)^{1/2} \frac{\rho\sigma_{\theta o}}{\rho_R^2\sigma_\theta} = -\frac{3}{2}\frac{\tau_w}{\tau_{wo}}\frac{1}{\rho_R} \xrightarrow{o} -\frac{3}{2\rho} \tag{B.1}$$

$$\frac{\partial\left(\tau_w/\tau_{wo}\right)}{\partial\sigma_\theta} = -\frac{3}{2}\left(\frac{\rho\sigma_{\theta o}}{\rho_R\sigma_\theta}\right)^{1/2} \frac{\rho\sigma_{\theta o}}{\rho_R\sigma_\theta^2} = -\frac{3}{2}\frac{\tau_w}{\tau_{wo}}\frac{1}{\sigma_\theta} \xrightarrow{o} -\frac{3}{2\sigma_{\theta o}} \tag{B.2}$$

$$\frac{\partial\Upsilon}{\partial\rho_R} = -K_\tau \frac{\partial\left(\tau_w/\tau_{wo}\right)}{\partial\rho_R} \xrightarrow{o} \frac{3K_\tau}{2\rho} = \frac{\bar{K}_\tau}{\rho} \tag{B.3}$$

$$\frac{\partial\Upsilon}{\partial\sigma_\theta} = K_\sigma \frac{\partial\left(\left(\sigma_\theta + \sigma_z\right)/\sigma_{Io}\right)}{\partial\sigma_\theta} - K_\tau \frac{\partial\left(\tau_w/\tau_{wo}\right)}{\partial\sigma_\theta} \xrightarrow{o} \frac{K_\sigma}{\sigma_{Io}} + \frac{3K_\tau}{2\sigma_{\theta o}} = \frac{\bar{K}_\sigma + \bar{K}_\tau}{\sigma_{\theta o}} \tag{B.4}$$

$$\frac{\partial \Upsilon}{\partial \sigma_z} = K_\sigma \frac{\partial \left(\left(\sigma_\theta + \sigma_z \right) / \sigma_{Io} \right)}{\partial \sigma_z} \xrightarrow{o} \frac{K_\sigma}{\sigma_{Io}} = \frac{\bar{K}_\sigma}{\sigma_{\theta o}} \tag{B.5}$$

$$\left. \frac{\partial \hat{S}_\theta^{act}}{\partial \rho_R} \right|_o = \left. \frac{d\hat{S}_\theta^{act}}{dC} \frac{dC}{d\left(\tau_w / \tau_{wo} \right)} \frac{\partial \left(\tau_w / \tau_{wo} \right)}{\partial \rho_R} \right|_o = \left. \frac{d\hat{S}_\theta^{act}}{dC} \right|_o \frac{3C_S}{2\rho} = \frac{c_{\theta\theta o}^{act}}{2\rho\phi_o^m} \tag{B.6}$$

$$\left. \frac{\partial \hat{S}_\theta^{act}}{\partial \sigma_\theta} \right|_o = \left. \frac{d\hat{S}_\theta^{act}}{dC} \frac{dC}{d\left(\tau_w / \tau_{wo} \right)} \frac{\partial \left(\tau_w / \tau_{wo} \right)}{\partial \sigma_\theta} \right|_o = \left. \frac{d\hat{S}_\theta^{act}}{dC} \right|_o \frac{3C_S}{2\sigma_{\theta o}} = \frac{c_{\theta\theta o}^{act}}{2\sigma_{\theta o}\phi_o^m} \tag{B.7}$$

Jacobian derivatives at original homeostatic state o

$$\left. \frac{1}{k_o} \frac{\partial \dot{\rho}_R}{\partial \rho_R} \right|_o = \frac{\rho - \rho_o^e}{\rho} \bar{K}_\tau \tag{B.8}$$

$$\left. \frac{1}{k_o} \frac{\partial \dot{\rho}_R}{\partial \sigma_\theta} \right|_o = \frac{\rho - \rho_o^e}{\sigma_{\theta o}} \left(\bar{K}_\sigma + \bar{K}_\tau \right) \tag{B.9}$$

$$\left. \frac{1}{k_o} \frac{\partial \dot{\rho}_R}{\partial \sigma_z} \right|_o = \frac{\rho - \rho_o^e}{\sigma_{\theta o}} \bar{K}_\sigma \tag{B.10}$$

$$\left. -\frac{\rho}{k_o \sigma_{\theta o}} \frac{\partial \dot{\sigma}_\theta}{\partial \rho_R} \right|_o = \left(2\frac{\sigma_{\theta o}^{ne}}{c_{\theta\theta o}} + \frac{\rho - \rho_o^e}{\rho} \right) \bar{K}_\tau + 2\frac{\sigma_{\theta o}^{ne}}{c_{\theta\theta o}} \frac{\rho_o^e}{\rho - \rho_o^e} + \frac{\mathcal{C}_{\theta\theta o}^{act}}{c_{\theta\theta o}} \tag{B.11}$$

$$\left. -\frac{1}{k_o} \frac{\partial \dot{\sigma}_\theta}{\partial \sigma_\theta} \right|_o = \left(2\frac{\sigma_{\theta o}^{ne}}{c_{\theta\theta o}} + \frac{\rho - \rho_o^e}{\rho} \right) \left(\bar{K}_\sigma + \bar{K}_\tau \right) - 2\frac{\sigma_{\theta o}^{ne}}{c_{\theta\theta o}} + \frac{\mathcal{C}_{\theta\theta o}^{act}}{c_{\theta\theta o}} \tag{B.12}$$

$$\left. -\frac{1}{k_o} \frac{\partial \dot{\sigma}_\theta}{\partial \sigma_z} \right|_o = \left(2\frac{\sigma_{\theta o}^{ne}}{c_{\theta\theta o}} + \frac{\rho - \rho_o^e}{\rho} \right) \bar{K}_\sigma \tag{B.13}$$

$$\begin{aligned} \left. -\frac{\rho}{k_o \sigma_{\theta o}} \frac{\partial \dot{\sigma}_z}{\partial \rho_R} \right|_o = & \left(\frac{c_{\theta zo}}{c_{\theta\theta o}} \frac{\sigma_{\theta o}^{ne}}{\sigma_{\theta o}} + \frac{\sigma_{zo}^e}{\sigma_{\theta o}} - \frac{\rho_o^e}{\rho} \frac{\sigma_{zo}}{\sigma_{\theta o}} \right) \bar{K}_\tau + \frac{c_{\theta zo}}{c_{\theta\theta o}} \frac{\sigma_{\theta o}^{ne}}{\sigma_{\theta o}} \frac{\rho_o^e}{\rho - \rho_o^e} \\ & + \left(\frac{\sigma_{zo}^e}{\sigma_{\theta o}} - \frac{\rho_o^e}{\rho} \frac{\sigma_{zo}}{\sigma_{\theta o}} \right) \frac{\rho}{\rho - \rho_o^e} + \frac{c_{\theta zo}}{2\sigma_{\theta o}} \frac{\mathcal{C}_{\theta\theta o}^{act}}{c_{\theta\theta o}} \end{aligned} \tag{B.14}$$

$$\left. -\frac{1}{k_o} \frac{\partial \dot{\sigma}_z}{\partial \sigma_\theta} \right|_o = \left(\frac{c_{\theta zo}}{c_{\theta\theta o}} \frac{\sigma_{\theta o}^{ne}}{\sigma_{\theta o}} + \frac{\sigma_{zo}^e}{\sigma_{\theta o}} - \frac{\rho_o^e}{\rho} \frac{\sigma_{zo}}{\sigma_{\theta o}} \right) \left(\bar{K}_\sigma + \bar{K}_\tau \right) + \frac{c_{\theta zo}}{2\sigma_{\theta o}} \frac{2\sigma_{\theta o}^{ne} + \mathcal{C}_{\theta\theta o}^{act}}{c_{\theta\theta o}} \tag{B.15}$$

$$\left. -\frac{1}{k_o} \frac{\partial \dot{\sigma}_z}{\partial \sigma_z} \right|_o = 1 + \left(\frac{c_{\theta zo}}{c_{\theta\theta o}} \frac{\sigma_{\theta o}^{ne}}{\sigma_{\theta o}} + \frac{\sigma_{zo}^e}{\sigma_{\theta o}} - \frac{\rho_o^e}{\rho} \frac{\sigma_{zo}}{\sigma_{\theta o}} \right) \bar{K}_\sigma \tag{B.16}$$